Computation of Maxwell singular solution by nodal-continuous elements

Huo-Yuan Duan[a], Roger C. E. Tan[b], Suh-Yuh Yang[c,*], Cheng-Shu You[c]

[a]*Collaborative Innovation Centre of Mathematics, School of Mathematics and Statistics, Wuhan University, Wuhan 430072, China*
[b]*Department of Mathematics, National University of Singapore, 2 Science Drive 2, Singapore 117543, Singapore*
[c]*Department of Mathematics, National Central University, Jhongli City, Taoyuan County 32001, Taiwan*

Abstract

In this paper, we propose and analyze a nodal-continuous and H^1-conforming finite element method for the numerical computation of Maxwell's equations, with singular solution in a fractional order Sobolev space $H^r(\Omega)$, where r may take any value in the most interesting interval $(0, 1)$. The key feature of the method is that mass-lumping linear finite element L^2 projections act on the curl and divergence partial differential operators so that the singular solution can be sought in a setting of $L^2(\Omega)$ space. We shall use the nodal-continuous linear finite elements, enriched with one element bubble in each element, to approximate the singular and non-H^1 solution. Discontinuous and nonhomogeneous media are allowed in the method. Some error estimates are given and a number of numerical experiments for source problems as well as eigenvalue problems are presented to illustrate the superior performance of the proposed method.

Keywords: Maxwell's equations, singular and non-H^1 solution, L^2 projection, nodal-continuous element, interface problem, eigenvalue problem

2000 MSC: 35Q61, 35J47, 65N30, 65N25

1. Introduction

In electromagnetism, the governing spatial partial differential operators are mainly the curl operator and the divergence (div) operator. As a mathematical foundation of electromagnetism, the well-known Maxwell's equations are the set of partial differential equations in terms of such two operators [15]. In general, these two characteristic operators behave rather differently from the gradient operator, although they are closely related with the latter. In fact, whenever the physical domain is nonsmooth, with re-entrant corners and/or edges on the boundary, the former would lead to singular solution of not being in the Sobolev space $H^1(\Omega)$, which is a Hilbert space of square integrable functions as well as the gradients. As a matter of fact, the singular solution belongs to a fractional order Sobolev space $H^r(\Omega)$ only, where the index r which stands for the regularity of the solution may take any value in the real interval $(0, 1)$. The $H^r(\Omega)$ space is an intermediate between the $L^2(\Omega)$ space and the $H^1(\Omega)$ space, where the $L^2(\Omega)$ space is a Hilbert space of square integrable functions. This case with singular solution is also particularly relevant in discontinuous, anisotropic and nonhomogeneous media. In most cases, the regularity of the Maxwell's solution is the one of the solution of the elliptic problem of Laplacian minus one, while the latter is well known in [33] to be less than two on nonsmooth domains (say, nonconvex polygons), so that the former is less than one. For more details, we refer the readers to, e.g., [2, 19, 22, 23, 24] and the references cited therein.

For such a low regularity solution, it is well known that the classical nodal-continuous finite element method fails in the plain curl/div formulation. The failure exhibits an incorrect convergence. In other words, the finite element solution converges, but it does not converge to the true solution in $H^r(\Omega)$ space with $r < 1$, but to a member of $H^1(\Omega)$ space instead; see [4, 10, 36, 40]. Such a strange phenomenon had been puzzling to the community of both mathematicians and engineers for a long while. Especially, an attempt is in vain to capture the unbounded singularity

*Corresponding author. Tel.: +886-3-4227151 extension 65130; fax: +886-3-4257379.
Email addresses: hyduan.math@whu.edu.cn (Huo-Yuan Duan), scitance@nus.edu.sg (Roger C. E. Tan), syyang@math.ncu.edu.tw (Suh-Yuh Yang), 100281001@cc.ncu.edu.tw (Cheng-Shu You)

of the solution by using more elements and finer meshes near the re-entrant corners where the singularity takes place. It turns out that, for $r < 1$, the $H^1(\Omega)$ space is not dense in $H^r(\Omega)$ under the plain curl/div formulation. That is to say, the plain curl/div formulation accounts for the failure. Actually, the plain curl/div formulation would result in a Dirichlet integral formulation for any H^1 functions (cf. Remark 2.1 below). The Dirichlet integral of the nodal-continuous (and H^1-conforming) finite element solution would enforce a convergence to a member of $H^1(\Omega)$ space; see [3, 4, 7, 9, 18, 35].

This fact directs the way out to the modification of the plain curl/div formulation. Indeed, if the nodal-continuous finite element problem is properly formulated, a correct approximation can be achieved. However, unexpectedly, until the last decade, several theoretically and numerically successful nodal-continuous finite element methods have been available, such as the weighted method [21], the H^{-1} least-squares method [6, 8, 11], the weighted dual-potential least-squares method [39], the weighted mixed method [14], and the L^2 projection method [25, 26, 28, 29, 27]. These methods were designed for different models from electromagnetism. The central idea for all these is to modify the plain curl/div formulation in either the continuous stage or the discrete stage. The resultant modification can reduce or even remove the actions on the solution from the curl and the div partial derivatives. With the effects from the curl and the div operators being weaken, the nodal-continuous finite element solution could correctly converge to the true and singular solution. Note that, the resultant curl/div formulation with the modifications will no longer lead to a Dirichlet integral (cf. Remark 2.1 below), even if the finite element function is nodal-continuous and H^1-conforming.

In this paper we shall propose a generalization of the L^2 projection method to the Maxwell's equations in two-dimensional bounded domain Ω, of the form

$$\mathbf{curl}\,\mu^{-1}\mathrm{curl}\,\mathbf{u} - \varepsilon\nabla\,\mathrm{div}\,\varepsilon\mathbf{u} - \lambda\varepsilon\mathbf{u} = \varepsilon\mathbf{f}. \tag{1.1}$$

The coefficients μ and ε may be discontinuous, anisotropic and nonhomogeneous, and the domain Ω may be nonsmooth with re-entrant corners and/or edges on the boundary. For such a system of Maxwell's equations, the solution may not have the H^1-regularity. The key technique is still to apply finite element L^2 projections to the curl and div operators, so that the solution can be sought in a setting of $L^2(\Omega)$ space. In essence, this type of L^2 projections mimics the distributional partial derivatives in the finite element spaces. Thus, the partial derivatives of the curl and div operators are transferred to the test functions. As is well known (see [16, 17]), the nodal-continuous finite element space is dense in any $L^2(\Omega)$ space and even in any $L^1(\Omega)$ space (A Sobolev space of Lebesgue integrable functions). Consequently, we can expect that the underlying nodal-continuous finite element method could produce an approximation of the singular solution in $H^r(\Omega)$ with $r < 1$. Note that the $H^r(\Omega)$ space is a trivial subspace of the $L^2(\Omega)$ space.

In the present paper, we develop this new nodal-continuous finite element method for (1.1) with suitable boundary conditions. In addition to the introduction of the mass-lumping linear finite element L^2 projections to the curl and div operators, we shall employ the nodal-continuous linear elements, enriched with one element bubble in each element (see, e.g., [30, 31, 37] and the references cited therein). We should remark that this approach is essentially a three-node nodal-continuous linear finite element method, since the element bubbles can be eliminated statically in advance (cf. Appendix A). As will be seen from a number of numerical experiments, this new method is capable of approximating the singular solution in $H^r(\Omega)$ space, where r can be any value in the most interesting interval $(0, 1)$. The new method is also suitable for discontinuous and nonhomogeneous media. In such cases, the solution would be prevalently more singular. In general, only some piecewise H^r-regularity can be available. We will provide error estimates for the case $\lambda < 0$, in which convergence and error bounds are established in the L^2 norm. This case was not dealt with before and the argument for this case can embody the most essential ingredients of the theory of the L^2 projection method.

Finally, we emphasize that there are many essential differences between the present nodal-continuous finite element method and our previous works [25, 26, 27, 28, 29]. In [25], we adopted local L^2 projections for both curl and div operators and the Maxwell's solution is required to lie in $H^r(\Omega)$ for $r > 1/2$. The work [28] studies discontinuous media, adopting local L^2 projection for curl operator while mass-lumping L^2 projection for div operator. Again, the regularity $r > 1/2$ of the Maxwell's solution is necessary in the error analysis. In addition, [27] focuses on the homogeneous media and [26] studies the first-order curl-div magnetostatic problem with continuous media. Notice that most of the above-mentioned works did not consider the associated eigenproblems. In contrast, [29] is devoted to study the eigenproblems, using local L^2 projections for both div and curl operators. However, the method in [29] still requires the singular eigenfunctions lying in $H^r(\Omega)$ for $r > 1/2$ and the discontinuous media are not studied.

The remainder of this paper is organized as follows. In Section 2, we recall the continuous problem in curlcurl-graddiv form, together with the plain curl/div variational formulation. Several representative models from computa-

tional electromagnetism are also briefly reviewed. The nodal-continuous finite element method is defined in Section 3, where two mass-lumping L^2 projections and the nodal-continuous finite element spaces are introduced. Error estimates for the case $\lambda < 0$ are provided in Section 4. Numerical results are presented in Section 5, with applications to the source and eigenvalue problems of Maxwell's equations, in homogeneous as well as discontinuous nonhomogeneous media. Finally, some concluding remarks are given in Section 6.

2. Continuous problem

In relation to the Cartesian coordinates (x, y), we consider a simply-connected Lipschitz bounded domain $\Omega \subset \mathbb{R}^2$ with boundary Γ. An example is the L-shaped domain, with an opening angle of $3\pi/2$. Other examples include the nonconvex polygons with re-entrant corners. Let $\boldsymbol{\tau}$ denote the unit tangential vector along boundary Γ. Further, let a real scalar parameter $\mu > 0$ and a real scalar (or matrix) parameter $\varepsilon > 0$ denote the magnetic permeability and the dielectric permittivity, respectively. Both μ and ε characterize the physical properties of the medium in Ω. Let $\mathbf{u} = (u_1, u_2)$ denote the unknown field, e.g., the magnetic induction. Then the source problem of the Maxwell's equations that we shall consider reads as follows: *Find* $\mathbf{u}$ *such that*

$$\begin{cases} \mathbf{curl}\,\mu^{-1}\mathrm{curl}\,\mathbf{u} - \varepsilon\nabla\,\mathrm{div}\,\varepsilon\mathbf{u} - \lambda\,\varepsilon\mathbf{u} = \varepsilon\mathbf{f} & \text{in } \Omega, \\ \mathbf{u}\cdot\boldsymbol{\tau} = 0, \quad \mathrm{div}\,\varepsilon\mathbf{u} = 0 & \text{on } \Gamma. \end{cases} \tag{2.1}$$

Here $\mathbf{f}$ is a given source function and λ is a given real or complex number. In this paper, λ is assumed to be real, just for convenience. For a vector-valued function $\mathbf{u} = (u_1, u_2)$, we define the curl operator on $\mathbf{u}$ as $\mathrm{curl}\,\mathbf{u} = \partial_x u_2 - \partial_y u_1$ and the div operator as $\mathrm{div}\,\mathbf{u} = \partial_x u_1 + \partial_y u_2$. For a scalar function ϕ, we define the curl operator on ϕ as $\mathbf{curl}\,\phi = (\partial_y\phi, -\partial_x\phi)$ and the gradient operator as $\nabla\phi = (\partial_x\phi, \partial_y\phi)$. The coefficients μ and ε may be discontinuous. In that case, let $\mathscr{P}$ denote a partition of Ω, such that $\Omega = \cup_{j=1}^{J}\Omega_j$ and we shall assume that μ and ε are piecewise positive constant functions, i.e.,

$$\mu|_{\Omega_j} = \mu_j > 0 \quad \text{and} \quad \varepsilon|_{\Omega_j} = \varepsilon_j > 0 \quad \text{for } 1 \le j \le J.$$

To formulate a variational statement of problem (2.1), we need to introduce some Hilbert spaces. First, let

$$L^2(\Omega) = \left\{ q : \Omega \to \mathbb{R} \text{ is Lebesgue measurable with } \int_\Omega |q|^2 < \infty \right\},$$

equipped with the L^2 inner product $(p, q) := \int_\Omega pq$ and the L^2 norm $\|q\|_0 := \sqrt{(q, q)}$. The vector L^2 space $(L^2(\Omega))^2$ will denote the product of two $L^2(\Omega)$ spaces. The corresponding L^2 inner product and the L^2 norm will be denoted by the same notations $(\cdot,\cdot)$ and $\|\cdot\|_0$, i.e., $(\mathbf{u}, \mathbf{v}) = \int_\Omega \mathbf{u}\cdot\mathbf{v}$ and $\|\mathbf{v}\|_0 = \sqrt{(\mathbf{v}, \mathbf{v})}$. We introduce a Hilbert space for the solution of (2.1) as follows:

$$U = \{\mathbf{v} \in (L^2(\Omega))^2 : \mathrm{curl}\,\mathbf{v} \in L^2(\Omega), \mathrm{div}\,\varepsilon\mathbf{v} \in L^2(\Omega), \mathbf{v}\cdot\boldsymbol{\tau}|_\Gamma = 0\}. \tag{2.2}$$

By Green's formula of integration by parts, problem (2.1) can be stated as the following plain curl/div variational problem: *Find* $\mathbf{u} \in U$ *such that*

$$(\mu^{-1}\mathrm{curl}\,\mathbf{u}, \mathrm{curl}\,\mathbf{v}) + (\mathrm{div}\,\varepsilon\mathbf{u}, \mathrm{div}\,\varepsilon\mathbf{v}) - \lambda\,(\varepsilon\mathbf{u}, \mathbf{v}) = (\varepsilon\mathbf{f}, \mathbf{v}) \quad \forall\mathbf{v} \in U, \tag{2.3}$$

where we assume that the source function $\mathbf{f} \in (L^2(\Omega))^2$.

Several representative models in computational electromagnetism are reviewed in [10]. With few modifications, one can easily see that all of them can be stated in the same plain curl/div variational bilinear form as in (2.3), while the right-hand side are different.

- *Case 1.* The time-harmonic Maxwell's equations with the angular frequency $\omega^2 > 0$, i.e.,

$$\mathbf{curl}\,\mathrm{curl}\,\mathbf{u} - \omega^2\,\mathbf{u} = \mathbf{J}, \quad \mathrm{div}\,\mathbf{u} = g \quad \text{in } \Omega, \quad \mathbf{u}\cdot\boldsymbol{\tau} = 0 \quad \text{on } \Gamma. \tag{2.4}$$

  Here and below $\mathbf{J}$ and g are given functions. Indeed, with $\mu = \varepsilon := 1$ and $\lambda := \omega^2$, the time-harmonic Maxwell's equations can be stated in the form (2.3), with the following formulation:

$$(\mathrm{curl}\,\mathbf{u}, \mathrm{curl}\,\mathbf{v}) + (\mathrm{div}\,\mathbf{u}, \mathrm{div}\,\mathbf{v}) - \lambda\,(\mathbf{u}, \mathbf{v}) = (\mathbf{J}, \mathbf{v}) + (g, \mathrm{div}\,\mathbf{v}) \quad \forall\mathbf{v} \in U. \tag{2.5}$$

Note that the boundary condition of $\operatorname{div}\mathbf{u}$ on Γ is not needed for (2.4), because of $\operatorname{div}\mathbf{u} = g$ in Ω.

Similarly, the following three cases can be dealt with in the same bilinear form as in (2.3), with some obvious modifications in the right-hand side.

- *Case 2.* The vector potential equations:

$$\mathbf{curl}\operatorname{curl}\mathbf{u} = \mathbf{J}, \quad \operatorname{div}\mathbf{u} = g \quad \text{in } \Omega, \quad \mathbf{u}\cdot\boldsymbol{\tau} = 0 \quad \text{on } \Gamma.$$

- *Case 3.* The time-discretization of the transient Maxwell's equations with the parameter $-\lambda > 0$ being inversely proportional to the time step:

$$\mathbf{curl}\operatorname{curl}\mathbf{u} - \lambda\mathbf{u} = \mathbf{J}, \quad \operatorname{div}\mathbf{u} = g \quad \text{in } \Omega, \quad \mathbf{u}\cdot\boldsymbol{\tau} = 0 \quad \text{on } \Gamma.$$

- *Case 4.* The curl-div magnetostatic problem:

$$\operatorname{curl}\mathbf{u} = \kappa, \quad \operatorname{div}\mathbf{u} = g \quad \text{in } \Omega, \quad \mathbf{u}\cdot\boldsymbol{\tau} = 0 \quad \text{on } \Gamma.$$

To obtain a curl/div variational problem similar to (2.3), one needs only to define the right-hand side as $(\kappa, \operatorname{curl}\mathbf{v}) + (g, \operatorname{div}\mathbf{v})$, $\lambda := 0$ and $\mu = \varepsilon := 1$.

Remark 2.1. We remark that in the case of $\varepsilon = 1$, the following Dirichlet integral holds (see [18]):

$$(\operatorname{curl}\mathbf{u}, \operatorname{curl}\mathbf{v}) + (\operatorname{div}\mathbf{u}, \operatorname{div}\mathbf{v}) = (\nabla\mathbf{u}, \nabla\mathbf{v}) \quad \forall \mathbf{u}, \mathbf{v} \in (H^1(\Omega))^2 \cap U,$$

where $(H^1(\Omega))^2 := H^1(\Omega)\times H^1(\Omega)$ and $H^1(\Omega) = \{q \in L^2(\Omega) : \nabla q \in (L^2(\Omega))^2\}$.

3. Discrete problem

In this section, we develop the new nodal-continuous and H^1-conforming finite element method for problem (2.1). First, we introduce the following two Hilbert spaces [1, 32, 40]:

$$H_0^1(\Omega) = \{q \in H^1(\Omega) : q|_\Gamma = 0\},$$

$$H_0(\operatorname{curl};\Omega) = \{\mathbf{v} \in (L^2(\Omega))^2 : \operatorname{curl}\mathbf{v} \in L^2(\Omega), \mathbf{v}\cdot\boldsymbol{\tau}|_\Gamma = 0\}.$$

Let $\mathscr{T}_h$ be a conforming triangulation of Ω into shape-regular triangles K [13, 16], where $h := \max_{K\in\mathscr{T}_h} h_K$ and h_K is the diameter of K. We also assume that $\mathscr{T}_h$ is conforming to the material interfaces, if any. On each K, we denote by $P_\ell(K)$ the space of polynomials of degree not greater than $\ell \geq 0$. The nodal basis functions of $P_1(K)$ are given by λ_i, $1 \leq i \leq 3$, associated with the three vertices of K. We introduce the element-bubble on K by $b_K := \lambda_1\lambda_2\lambda_3$. Moreover, we define the bubble function space

$$B_h = \{\mathbf{v} \in (H_0^1(\Omega))^2 : \mathbf{v}|_K \in b_K(P_0(K))^2, \forall K \in \mathscr{T}_h\}, \tag{3.1}$$

and define the nodal-continuous linear finite element space

$$V_h = \{q \in H^1(\Omega) : q|_K \in P_1(K), K \in \mathscr{T}_h\}. \tag{3.2}$$

We then introduce the nodal-continuous and H^1-conforming finite element space U_h for the solution of problem (2.1) as follows:

$$U_h = ((V_h)^2 \cap H_0(\operatorname{curl};\Omega)) + B_h. \tag{3.3}$$

That is, for any $\mathbf{v}_h \in U_h$, $\mathbf{v}_h|_K \in (P_1^+(K))^2 := (P_1(K) + b_K P_0(K))^2$ on any $K \in \mathscr{T}_h$ and it can be written as the following sum:

$$\mathbf{v}_h = \sum_{i=1}^{3} \mathbf{c}_i\lambda_i + \mathbf{c}_K b_K,$$

where $\mathbf{c}_i, \mathbf{c}_K$ represent coefficients. Note that U_h is nonconforming to U. In fact, the $\operatorname{div} \varepsilon \mathbf{v}_h$ is generally not well-defined for $\mathbf{v}_h \in U_h$.

Additionally, we define the nodal-continuous and H^1-conforming finite element spaces Q_h and W_h for defining L^2 projections for the curl and the div operators as follows:

$$Q_h = V_h \cap H_0^1(\Omega), \tag{3.4}$$

$$W_h = V_h. \tag{3.5}$$

Over Q_h, we introduce the discrete L^2 inner product $(\cdot,\cdot)_{0,h}$ which is defined as

$$(p,q)_{0,h} = \sum_{K\in\mathscr{T}_h} \frac{|K|}{3} \sum_{i=1}^{3} p(a_i)q(a_i) \quad \forall p, q \in Q_h, \tag{3.6}$$

where $|K|$ is the area of K, and a_i, $1 \le i \le 3$, are the vertices of K. This discrete L^2 inner product $(p,q)_{0,h}$ is the so-called mass-lumping approximation of the usual L^2 inner product (p,q), see [43]. Note that the matrix generated from (3.6) is diagonal. On the other hand, we introduce the following discrete μ-weighted L^2 inner product $(\cdot,\cdot)_{0,\mu,h}$ over W_h as

$$(w,z)_{0,\mu,h} = \sum_{K\in\mathscr{T}_h} \frac{|K|}{3} \sum_{i=1}^{3} \mu w(a_i)z(a_i) \quad \forall w, z \in W_h. \tag{3.7}$$

Note that μ is a piecewise constant over Ω. The resultant matrix for (3.7) is still diagonal. In fact, (3.7) is a mass-lumping approximation of the μ-weighted L^2 inner product

$$(w,z)_{0,\mu} = \int_\Omega \mu w z.$$

Next, for any given $\mathbf{v} \in (L^2(\Omega))^2$, we define the projections $\check{R}_h(\operatorname{div} \varepsilon\mathbf{v}) \in Q_h$ and $R_h(\mu^{-1}\operatorname{curl} \mathbf{v}) \in W_h$ as follows:

$$(\check{R}_h(\operatorname{div} \varepsilon\mathbf{v}), q)_{0,h} = -(\mathbf{v}, \varepsilon\nabla q) \quad \forall q \in Q_h, \tag{3.8}$$

$$(R_h(\mu^{-1}\operatorname{curl} \mathbf{v}), w)_{0,\mu,h} = (\mathbf{v}, \mathbf{curl}\, w) \quad \forall w \in W_h. \tag{3.9}$$

Note that $\check{R}_h(\operatorname{div} \varepsilon\mathbf{v})$ and $R_h(\mu^{-1}\operatorname{curl} \mathbf{v})$ are not genuine L^2 projections of $\operatorname{div} \varepsilon\mathbf{v}$ and $\mu^{-1}\operatorname{curl} \mathbf{v}$. This is because the inner products are different from both sides of (3.8) and (3.9), and because $\operatorname{div} \varepsilon\mathbf{v}$ and $\mu^{-1}\operatorname{curl} \mathbf{v}$ are not necessarily L^2 functions. On the other hand, due to the fact that $(\cdot,\cdot)_{0,h}$ and $(\cdot,\cdot)_{0,\mu,h}$ are the approximations of the L^2 inner product $(\cdot,\cdot)$ and the μ-weighted L^2 inner product $(\cdot,\cdot)_{0,\mu}$, whenever $\mathbf{v} \in U$, $\check{R}_h(\operatorname{div} \varepsilon\mathbf{v})$ and $R_h(\mu^{-1}\operatorname{curl} \mathbf{v})$ are approximately L^2 projections of $\operatorname{div} \varepsilon\mathbf{v}$ and $\mu^{-1}\operatorname{curl} \mathbf{v}$, respectively. In fact, if replacing $(\cdot,\cdot)_{0,h}$ and $(\cdot,\cdot)_{0,\mu,h}$ by $(\cdot,\cdot)$ and $(\cdot,\cdot)_{0,\mu}$, both $\check{R}_h(\operatorname{div} \varepsilon\mathbf{v})$ and $R_h(\mu^{-1}\operatorname{curl} \mathbf{v})$ become the genuine L^2 projections of $\mathbf{v} \in U$. That is, when $\mathbf{v} \in U$, we have

$$(\check{R}_h(\operatorname{div} \varepsilon\mathbf{v}), q)_{0,h} = (\operatorname{div} \varepsilon\mathbf{v}, q) \quad \forall q \in Q_h,$$

$$(R_h(\mu^{-1}\operatorname{curl} \mathbf{v}), w)_{0,\mu,h} = (\mu^{-1}\operatorname{curl} \mathbf{v}, w)_{0,\mu} \quad \forall w \in W_h.$$

We remark that (3.8) and (3.9) are well-defined for all $\mathbf{v} \in (L^2(\Omega))^2$ and even for all $\mathbf{v} \in (L^1(\Omega))^2$, whatever μ and ε are discontinuous throughout Ω. The reason lies in that the curl and div partial derivatives have been transferred to apply to the test finite element spaces Q_h and W_h. In other words, both $\check{R}_h(\operatorname{div} \varepsilon\mathbf{v})$ and $R_h(\mu^{-1}\mathbf{curl}\, \mathbf{v})$ mimic the the distributional div and curl operators which are defined in the following way. Let $\mathscr{D}(\Omega) := C_0^\infty(\Omega)$, the space of infinitely differentiable functions with compact supports in Ω. Denote by $\mathscr{D}'(\Omega)$ the dual of $\mathscr{D}(\Omega)$. For a given $\mathbf{v} \in (L^1(\Omega))^2$, the distributional $\operatorname{div} \varepsilon\mathbf{v} \in \mathscr{D}'(\Omega)$ and $\operatorname{curl} \mathbf{v} \in \mathscr{D}'(\Omega)$ are respectively defined by

$$\langle \operatorname{div} \varepsilon\mathbf{v}, q\rangle = -\int_\Omega \mathbf{v} \cdot \varepsilon\nabla q \quad \forall q \in \mathscr{D}(\Omega),$$

$$\langle \operatorname{curl} \mathbf{v}, z\rangle = \int_\Omega \mathbf{v} \cdot \mathbf{curl}\, z \quad \forall z \in \mathscr{D}(\Omega).$$

$u_{1h}|_K \in P_1^+(K)$ $\qquad$ $u_{2h}|_K \in P_1^+(K)$

Figure 3.1. Degrees of freedom of $\mathbf{u}_h = (u_{1h}, u_{2h})$ on K.

$\breve{R}_h(\operatorname{div} \varepsilon \mathbf{u}_h)|_K \in P_1(K)$ $\qquad$ $R_h(\mu^{-1}\operatorname{curl} \mathbf{u}_h)|_K \in P_1(K)$

Figure 3.2. Degrees of freedom of $\breve{R}_h(\operatorname{div} \varepsilon \mathbf{u}_h)$ and $R_h(\mu^{-1}\operatorname{curl} \mathbf{u}_h)$ on K.

Now, the nodal-continuous and H^1-conforming finite element method for problem (2.1) that we consider can be posed as follows: *Find* $\mathbf{u}_h \in U_h$ *such that*

$$\mathcal{A}_h(\mathbf{u}_h, \mathbf{v}_h) = (\varepsilon \mathbf{f}, \mathbf{v}_h) \quad \forall \mathbf{v}_h \in U_h, \tag{3.10}$$

where the bilinear form $\mathcal{A}_h(\cdot, \cdot)$ is given by

$$\mathcal{A}_h(\mathbf{u}_h, \mathbf{v}_h) := (R_h(\mu^{-1}\operatorname{curl} \mathbf{u}_h), R_h(\mu^{-1}\operatorname{curl} \mathbf{v}_h))_{0,\mu,h} + (\breve{R}_h(\operatorname{div} \varepsilon \mathbf{u}_h), \breve{R}_h(\operatorname{div} \varepsilon \mathbf{v}_h))_{0,h} - \lambda\, (\varepsilon \mathbf{u}_h, \mathbf{v}_h), \tag{3.11}$$

which is obviously symmetric whenever the real parameter ε is a scalar or a symmetric matrix. The proposed method (3.10) is nonconforming, not only because the bilinear form is nonconforming to the plain curl/div bilinear form in (2.3), but also because of the nonconformity of U_h in U. We should emphasize that U_h is always globally continuous throughout Ω, no matter if μ and ε are continuous or discontinuous. In addition, since the element-bubbles in U_h can be statically eliminated at element levels, (3.10) is in essence a nodal-continuous linear finite element method (see Appendix A for more details). Note that $\mathbf{u}_h \in U_h$ actually satisfies $\mathbf{u}_h|_K \in (P_1^+(K))^2 := (P_1(K) + b_K P_0(K))^2$ for all $K \in \mathscr{T}_h$, so the degrees of freedom of $\mathbf{u}_h = (u_{1h}, u_{2h})$ on an element K are illustrated in Figure 3.1. For convenience, the degrees of freedom for the computations of the L^2 projections $\breve{R}_h(\operatorname{div} \varepsilon \mathbf{u}_h) \in Q_h$ and $R_h(\mu^{-1}\operatorname{curl} \mathbf{u}_h) \in W_h$ on an element K are also illustrated in Figure 3.2.

From projections (3.8) and (3.9), we have seen that (3.11) makes sense even if the solution is in $(L^2(\Omega))^2$ space only. It is then expected that for all $r \in (0, 1)$, method (3.10) can give a correctly convergent nodal-continuous finite element solution. The convergence rate can be expected to be $O(h^r)$ in the L^2 norm, if the exact solution $\mathbf{u} \in \prod_{j=1}^{J} (H^r(\Omega_j))^2$. This prediction will be verified in Section 4 for the case $\lambda < 0$. We also refer the readers to [27] for some theoretical analyses for the homogeneous case of $\mu = \varepsilon = 1$. Numerical results reported in Section 5 will illustrate the superior performance of the proposed method (3.10).

The finite element method (3.10) will lead to a sparse linear algebraic system. In addition, if the real parameter ε is a scalar or a symmetric matrix, then the resulting linear system will be symmetric. We now give some implementation details of how the linear system is assembled. Let $\{\eta_1, \eta_2, \cdots, \eta_{n_q}\}$ be a basis of Q_h, $\{\chi_1, \chi_2, \cdots, \chi_{n_w}\}$ a basis of W_h, and $\{\boldsymbol{\varphi}_1, \boldsymbol{\varphi}_2, \cdots, \boldsymbol{\varphi}_{n_u}\}$ a basis of U_h. Then the finite element solution $\mathbf{u}_h \in U_h$ and the test function $\mathbf{v}_h \in U_h$ in (3.10) can be respectively expressed as

$$\mathbf{u}_h = \sum_{i=1}^{n_u} a_i \boldsymbol{\varphi}_i \quad \text{and} \quad \mathbf{v}_h = \sum_{i=1}^{n_u} b_i \boldsymbol{\varphi}_i.$$

We denote $\boldsymbol{a} := (a_1, a_2, \cdots, a_{n_u})^\top \in \mathbb{R}^{n_u}$ and $\boldsymbol{b} := (b_1, b_2, \cdots, b_{n_u})^\top \in \mathbb{R}^{n_u}$. First, let us consider the first term in (3.11). Since $R_h(\mu^{-1}\mathrm{curl}\ \mathbf{v}_h) \in W_h$, it can be written as $R_h(\mu^{-1}\mathrm{curl}\ \mathbf{v}_h) = \sum_{k=1}^{n_w} \widehat{b}_k \chi_k$ for some $\widehat{\boldsymbol{b}} := (\widehat{b}_1, \widehat{b}_2, \cdots, \widehat{b}_{n_w})^\top$. From (3.9), for any $w = \sum_{j=1}^{n_w} \widehat{w}_j \chi_j \in W_h$ with $\widehat{\boldsymbol{w}} := (\widehat{w}_1, \widehat{w}_2, \cdots, \widehat{w}_{n_w})^\top \in \mathbb{R}^{n_w}$, we have

$$\widehat{\boldsymbol{w}}^\top \mathbf{A}_1 \widehat{\boldsymbol{b}} = \widehat{\boldsymbol{w}}^\top \mathbf{C} \boldsymbol{b}, \tag{3.12}$$

where the entries of the matrices $\mathbf{A}_1 = (\mathbf{A}_{1jk}) \in \mathbb{R}^{n_w \times n_w}$ and $\mathbf{C} = (\mathbf{C}_{ji}) \in \mathbb{R}^{n_w \times n_u}$ are respectively given by

$$\mathbf{A}_{1jk} = (\chi_k, \chi_j)_{0,\mu,h} \quad \text{for } j,k = 1, 2, \cdots, n_w,$$

$$\mathbf{C}_{ji} = (\boldsymbol{\varphi}_i, \mathbf{curl}\, \chi_j) \quad \text{for } j = 1, 2, \cdots, n_w,\ i = 1, 2, \cdots, n_u.$$

Since $w \in W_h$ can be arbitrarily chosen, (3.12) holds for all $\widehat{\boldsymbol{w}} \in \mathbb{R}^{n_w}$. This leads to

$$\widehat{\boldsymbol{b}} = \mathbf{A}_1^{-1} \mathbf{C} \boldsymbol{b}. \tag{3.13}$$

Note that matrix $\mathbf{C}$ is sparse, and matrix $\mathbf{A}_1$ is diagonal because it is generated from the mass-lumping approximation (3.7). Combining the fact $R_h(\mu^{-1}\mathrm{curl}\ \mathbf{v}_h) \in W_h$ with (3.9) and (3.13), the first term in (3.11) can be reformulated as

$$(R_h(\mu^{-1}\mathrm{curl}\ \mathbf{u}_h), R_h(\mu^{-1}\mathrm{curl}\ \mathbf{v}_h))_{0,\mu,h} = (\mathbf{u}_h, \mathbf{curl}\, R_h(\mu^{-1}\mathrm{curl}\ \mathbf{v}_h)) = \widehat{\boldsymbol{b}}^\top \mathbf{C} \boldsymbol{a} = \boldsymbol{b}^\top \mathbf{C}^\top \mathbf{A}_1^{-1} \mathbf{C} \boldsymbol{a}. \tag{3.14}$$

Next, we consider the second term in (3.11). Let $\breve{R}_h(\mathrm{div}\ \varepsilon \mathbf{v}_h) = \sum_{k=1}^{n_q} \breve{b}_k \eta_k \in Q_h$ for some $\breve{\boldsymbol{b}} := (\breve{b}_1, \breve{b}_2, \cdots, \breve{b}_{n_q})^\top \in \mathbb{R}^{n_q}$. From (3.8), for any $q = \sum_{j=1}^{n_q} \breve{q}_j \eta_j \in Q_h$ with $\breve{\boldsymbol{q}} := (\breve{q}_1, \breve{q}_2, \cdots, \breve{q}_{n_q})^\top \in \mathbb{R}^{n_q}$, we have

$$\breve{\boldsymbol{q}}^\top \mathbf{A}_2 \breve{\boldsymbol{b}} = \breve{\boldsymbol{q}}^\top \mathbf{D} \boldsymbol{b}, \tag{3.15}$$

where the entries of the matrices $\mathbf{A}_2 = (\mathbf{A}_{2jk}) \in \mathbb{R}^{n_q \times n_q}$ and $\mathbf{D} = (\mathbf{D}_{ji}) \in \mathbb{R}^{n_q \times n_u}$ are respectively defined by

$$\mathbf{A}_{2jk} = (\eta_k, \eta_j)_{0,h} \quad \text{for } j,k = 1, 2, \cdots, n_q,$$

$$\mathbf{D}_{ji} = -(\boldsymbol{\varphi}_i, \varepsilon \nabla \eta_j) \quad \text{for } j = 1, 2, \cdots, n_q,\ i = 1, 2, \cdots, n_u.$$

Similarly, since (3.15) holds for all $\breve{\boldsymbol{q}} \in \mathbb{R}^{n_q}$, we obtain

$$\breve{\boldsymbol{b}} = \mathbf{A}_2^{-1} \mathbf{D} \boldsymbol{b}, \tag{3.16}$$

where $\mathbf{D}$ is a sparse matrix and, due to the mass-lumping approximation (3.6), $\mathbf{A}_2$ is diagonal. Now, since $\breve{R}_h(\mathrm{div}\ \varepsilon \mathbf{v}_h) \in Q_h$, with (3.8) and (3.16), we can rewrite the second term in (3.11) as

$$(\breve{R}_h(\mathrm{div}\ \varepsilon \mathbf{u}_h), \breve{R}_h(\mathrm{div}\ \varepsilon \mathbf{v}_h))_{0,h} = -(\mathbf{u}_h, \varepsilon \nabla \breve{R}_h(\mathrm{div}\ \varepsilon \mathbf{v}_h)) = \breve{\boldsymbol{b}}^\top \mathbf{D} \boldsymbol{a} = \boldsymbol{b}^\top \mathbf{D}^\top \mathbf{A}_2^{-1} \mathbf{D} \boldsymbol{a}. \tag{3.17}$$

The last term in (3.11) and the right-hand side of (3.10) can be easily represented by

$$-\lambda(\varepsilon \mathbf{u}_h, \mathbf{v}_h) = -\boldsymbol{b}^\top \mathbf{M} \boldsymbol{a}, \tag{3.18}$$

where the entries of the matrix $\mathbf{M} = (\mathbf{M}_{ij}) \in \mathbb{R}^{n_u \times n_u}$ are defined as

$$\mathbf{M}_{ij} = \lambda(\varepsilon \boldsymbol{\varphi}_j, \boldsymbol{\varphi}_i) \quad \text{for } i,j = 1, 2, \cdots, n_u,$$

and

$$(\varepsilon \mathbf{f}, \mathbf{v}_h) = \boldsymbol{b}^\top \mathbf{F} \tag{3.19}$$

with the vector $\mathbf{F} = (\mathbf{F}_i) \in \mathbb{R}^{n_u}$ given by

$$\mathbf{F}_i = (\varepsilon \mathbf{f}, \boldsymbol{\varphi}_i) \quad \text{for } i = 1, 2, \cdots, n_u.$$

As the last step, combining (3.14), (3.17), (3.18) and (3.19) yields the following algebraic system:

$$\boldsymbol{b}^\top\Big(\mathbf{C}^\top\mathbf{A}_1^{-1}\mathbf{C}+\mathbf{D}^\top\mathbf{A}_2^{-1}\mathbf{D}-\mathbf{M}\Big)\boldsymbol{a}=\boldsymbol{b}^\top\mathbf{F},$$

which, since $\boldsymbol{b}$ can be arbitrarily chosen from $\mathbb{R}^{n_u}$, implies the sparse linear system,

$$\Big(\mathbf{C}^\top\mathbf{A}_1^{-1}\mathbf{C}+\mathbf{D}^\top\mathbf{A}_2^{-1}\mathbf{D}-\mathbf{M}\Big)\boldsymbol{a}=\mathbf{F}. \tag{3.20}$$

Once we solve this linear system for the unknown vector $\boldsymbol{a}$, we obtain equivalently the finite element solution $\mathbf{u}_h$ of problem (3.10).

To conclude this section, we give a brief remark on the associated eigenvalue problem. Indeed, we can further consider the Maxwell eigenvalue problem posed as follows: *Find* $\omega^2\in\mathbb{R}$ *and* $\mathbf{u}\in U$ *such that*

$$\mathbf{curl}\,\mu^{-1}\mathrm{curl}\,\mathbf{u}-\varepsilon\nabla\,\mathrm{div}\,\varepsilon\mathbf{u}=\omega^2\varepsilon\mathbf{u}\quad\text{in }\Omega,\quad \mathbf{u}\cdot\boldsymbol{\tau}=0,\quad \mathrm{div}\,\varepsilon\mathbf{u}=0\quad\text{on }\Gamma. \tag{3.21}$$

An example from computational electromagnetism is to find $\omega^2\in\mathbb{R}$ and $\mathbf{u}\in U$ such that

$$\mathbf{curl}\,\mu^{-1}\mathrm{curl}\,\mathbf{u}=\omega^2\varepsilon\mathbf{u},\quad \mathrm{div}\,\varepsilon\mathbf{u}=0\quad\text{in }\Omega,\quad \mathbf{u}\cdot\boldsymbol{\tau}=0\quad\text{on }\Gamma. \tag{3.22}$$

When applied to the corresponding eigenvalue problem, the proposed finite element method can produce correctly convergent finite element eigenvalues, with convergence rate of $O(h^{2r})$, whenever the corresponding eigenfunctions are of $\prod_{j=1}^{J}(H^r(\Omega_j))^2$ (cf. [29]). In addition, there are some eigenvalues for which the eigenfunctions belong to $\prod_{j=1}^{J}(H^1(\Omega_j))^2$ and even more regular. For these eigenvalues, the theoretical convergence rate is at most $O(h^2)$. This is because the linear finite elements are only used and because there exist consistency errors due to the replacements of the L^2 inner product $(\cdot,\cdot)$ and the μ-weighted L^2 inner product $(\cdot,\cdot)_{0,\mu}$ by the discrete L^2 inner products $(\cdot,\cdot)_{0,h}$ and $(\cdot,\cdot)_{0,\mu,h}$. The correctness of this assertion is supported by the numerical results given in Section 5.

4. Error estimates

In this section, we derive error estimates for the finite element solution of (3.10). For simplicity, we consider the case $\lambda<0$. On the one hand, this case was not dealt with before, and on the other hand, the argument for this case can embody the most essential ingredients of the theory of the L^2 projection method. The error estimates consist of two parts, one is the consistent errors from the L^2 projections and the other is the finite element interpolation errors.

We introduce some notations of Sobolev spaces [1]. As usual, for any $D\subset\Omega$, $\|\cdot\|_{t,D}$ denotes the norm of $H^t(D)$, where $t\in\mathbb{R}$. For $t=0$, $H^0(D)=L^2(D)$. For $t=1$, we will use $|q|_{1,D}=\|\nabla q\|_{0,D}$ for $q\in H^1(D)$. When $D=\Omega$, the subscript D will be omitted.

Since $\lambda<0$, the following coercivity

$$\mathcal{A}_h(\mathbf{v}_h,\mathbf{v}_h)\geq c\Big(\|\mathbf{v}_h\|_0^2+\|R_h(\mu^{-1}\mathrm{curl}\,\mathbf{v}_h)\|_{0,\mu,h}^2+\|\check{R}_h(\mathrm{div}\,\varepsilon\mathbf{v}_h)\|_{0,h}^2\Big) \tag{4.1}$$

holds trivially for all $\mathbf{v}_h\in U_h$. This ensures the existence and uniqueness of the finite element solution $\mathbf{u}_h\in U_h$ to (3.10). Regarding the discrete L^2 inner product $(\cdot,\cdot)_{0,h}$ and the nodal-continuous linear finite element space Q_h, from [16, 43] we have

$$\|q_h\|_{0,h}\leq c\|q_h\|_0,\quad \|q_h\|_0\leq c\|q_h\|_{0,h}\quad\forall q_h\in Q_h, \tag{4.2}$$

$$|(p_h,q_h)-(p_h,q_h)_{0,h}|\leq ch\|p_h\|_1\|q_h\|_0\quad\forall p_h,q_h\in Q_h. \tag{4.3}$$

Similar results hold for the discrete μ-weighted L^2 inner product $(\cdot,\cdot)_{0,\mu,h}$ and the nodal-continuous linear finite element space W_h.

Let $\mathbf{u}$ be the exact solution of the Maxwell's problem (2.1). From (3.8), (3.9), (3.10) and (2.1), we have

$$\begin{aligned}\mathcal{A}_h(\mathbf{u}-\mathbf{u}_h,\mathbf{v}_h) &= (\mu^{-1}\mathrm{curl}\,\mathbf{u},R_h(\mu^{-1}\mathrm{curl}\,\mathbf{v}_h))_{0,\mu}-(\mu^{-1}\mathrm{curl}\,\mathbf{u},\mu^{-1}\mathrm{curl}\,\mathbf{v}_h)_{0,\mu}\\ &\quad+(\mathrm{div}\,\varepsilon\mathbf{u},\check{R}_h(\mathrm{div}\,\varepsilon\mathbf{v}_h))+(\varepsilon\nabla\mathrm{div}\,\varepsilon\mathbf{u},\mathbf{v}_h)\quad\forall\mathbf{v}_h\in U_h.\end{aligned} \tag{4.4}$$

Put

$$w:=\mu^{-1}\mathrm{curl}\,\mathbf{u},\quad p:=\mathrm{div}\,\varepsilon\mathbf{u}. \tag{4.5}$$

It follows from (2.1) that $w \in H^1(\Omega)$ and $p \in H_0^1(\Omega)$. Let $\widetilde{w} \in W_h$ and $\widetilde{p} \in Q_h$ denote their finite element interpolations. If $w \in H^1(\Omega) \cap \prod_{j=1}^J H^{1+r}(\Omega_j)$ and $p \in H_0^1(\Omega) \cap \prod_{j=1}^J H^{1+r}(\Omega_j)$, $r \in (0,1)$, from the standard finite element interpolation theory [13, 16, 17, 42], we find that

$$\|\widetilde{w} - w\|_0 + h|\widetilde{w} - w|_1 \le ch^{1+r} \sum_{j=1}^J \|w\|_{1+r,\Omega_j}, \tag{4.6}$$

$$\|\widetilde{p} - p\|_0 + h|\widetilde{p} - p|_1 \le ch^{1+r} \sum_{j=1}^J \|p\|_{1+r,\Omega_j}. \tag{4.7}$$

Now, we can give the bound of $\mathcal{A}_h(\mathbf{u} - \mathbf{u}_h, \mathbf{v}_h)$. Introduce the energy norm $|||\cdot|||_h$ on U_h by

$$|||\mathbf{v}_h|||_h^2 := \|\mathbf{v}_h\|_0^2 + \|R_h(\mu^{-1}\mathrm{curl}\,\mathbf{v}_h)\|_{0,\mu,h}^2 + \|\breve{R}_h(\mathrm{div}\,\varepsilon\mathbf{v}_h)\|_{0,h}^2. \tag{4.8}$$

Lemma 4.1. *Assume that $w \in H^1(\Omega) \cap \prod_{j=1}^J H^{1+r}(\Omega_j)$ and $p \in H_0^1(\Omega) \cap \prod_{j=1}^J H^{1+r}(\Omega_j)$, $r \in (0,1)$. Then we have*

$$\mathcal{A}_h(\mathbf{u} - \mathbf{u}_h, \mathbf{v}_h) \le ch^r\Big(\|w\|_1 + \|p\|_1 + \sum_{j=1}^J \|w\|_{1+r,\Omega_j} + \sum_{j=1}^J \|p\|_{1+r,\Omega_j}\Big)|||\mathbf{v}_h|||_h \quad \forall \mathbf{v}_h \in U_h. \tag{4.9}$$

Proof. From (4.4), (3.8) and (3.9), we have

$$\begin{aligned} \mathcal{A}_h(\mathbf{u} - \mathbf{u}_h, \mathbf{v}_h) \;=\; & (w - \widetilde{w}, R_h(\mu^{-1}\mathrm{curl}\,\mathbf{v}_h))_{0,\mu} + (\widetilde{w}, R_h(\mu^{-1}\mathrm{curl}\,\mathbf{v}_h))_{0,\mu} - (\widetilde{w}, R_h(\mu^{-1}\mathrm{curl}\,\mathbf{v}_h))_{0,\mu,h} \\ & + (\widetilde{w} - w, \mu^{-1}\mathrm{curl}\,\mathbf{v}_h)_{0,\mu} + (p - \widetilde{p}, \breve{R}_h(\mathrm{div}\,\varepsilon\mathbf{v}_h)) + (\widetilde{p}, \breve{R}_h(\mathrm{div}\,\varepsilon\mathbf{v}_h)) \\ & - (\widetilde{p}, \breve{R}_h(\mathrm{div}\,\varepsilon\mathbf{v}_h))_{0,h} + (\varepsilon\nabla(p - \widetilde{p}), \mathbf{v}_h), \end{aligned} \tag{4.10}$$

where

$$(w - \widetilde{w}, R_h(\mu^{-1}\mathrm{curl}\,\mathbf{v}_h))_{0,\mu} \le ch\|w\|_1\|R_h(\mu^{-1}\mathrm{curl}\,\mathbf{v}_h)\|_{0,\mu,h},$$

$$(\widetilde{w}, R_h(\mu^{-1}\mathrm{curl}\,\mathbf{v}_h))_{0,\mu} - (\widetilde{w}, R_h(\mu^{-1}\mathrm{curl}\,\mathbf{v}_h))_{0,\mu,h} \le ch\|w\|_1\|R_h(\mu^{-1}\mathrm{curl}\,\mathbf{v}_h)\|_{0,\mu,h},$$

$$(\widetilde{w} - w, \mu^{-1}\mathrm{curl}\,\mathbf{v}_h)_{0,\mu} \le ch^r \sum_{j=1}^J \|w\|_{1+r,\Omega_j}\|\mathbf{v}_h\|_0.$$

Similar results hold for the remaining parts of p in (4.10). The proof is completed. □

In what follows, we shall construct a finite element interpolation $\widetilde{\mathbf{u}} \in U_h$ to the exact solution $\mathbf{u}$ such that

$$\|R_h(\mu^{-1}\mathrm{curl}\,(\mathbf{u} - \widetilde{\mathbf{u}}))\|_{0,\mu,h} = \|\breve{R}_h(\mathrm{div}\,\varepsilon(\mathbf{u} - \widetilde{\mathbf{u}}))\|_{0,h} = 0 \tag{4.11}$$

and

$$\|\mathbf{u} - \widetilde{\mathbf{u}}\|_0 \le ch^r \sum_{j=1}^J \|\mathbf{u}\|_{r,\Omega_j}. \tag{4.12}$$

The equalities in (4.11) are the key ingredients for the L^2 projected terms $R_h(\mu^{-1}\mathrm{curl}\,(\mathbf{u} - \widetilde{\mathbf{u}}))$ and $\breve{R}_h(\mathrm{div}\,\varepsilon(\mathbf{u} - \widetilde{\mathbf{u}}))$ to yield *zero* errors only. Otherwise, the proposed method cannot produce a correctly convergent nodal-continuous finite element solution whenever the exact solution does not belong to $H^1(\Omega)$. Note that the standard finite element interpolation of $\mathbf{u}$ can satisfy (4.12), but (4.11) is not necessarily fulfilled. This is why we enrich the linear element space $(V_h)^2 \cap H_0(\mathrm{curl}\,;\Omega)$ with an element-bubble space B_h, so that we can have (4.11). To establish (4.11), we shall also make use of the following trivial inclusions:

$$\mathrm{curl}\,P_1(K), \quad \varepsilon|_K\nabla P_1(K) \subset (P_0(K))^2. \tag{4.13}$$

Lemma 4.2. *For $\mathbf{u} \in \prod_{j=1}^J (H^r(\Omega_j))^2$, $r \in (0,1)$, there exists $\widetilde{\mathbf{u}} \in U_h$ such that (4.11) and (4.12) hold.*

Proof. From the standard finite element interpolation, there exists $\mathbf{u}^0 \in (V_h)^2 \cap H_0(\mathrm{curl}\,;\Omega)$ such that (4.12) holds, i.e.,

$$\|\mathbf{u} - \mathbf{u}^0\|_0 \le ch^r \sum_{j=1}^{J} \|\mathbf{u}\|_{r,\Omega_j}.$$

We now construct the desired $\widetilde{\mathbf{u}} \in U_h$ in the following way. On K, we write

$$\widetilde{\mathbf{u}} = \mathbf{u}^0 + \sum_{K\in\mathscr{T}_h} \mathbf{c}_K b_K,$$

where $\mathbf{c}_K$ is to be determined so that (4.12) holds. Since $b_K \in H_0^1(K)$, it can be easily verified that $\widetilde{\mathbf{u}}$ can be uniquely determined by requiring that

$$\widetilde{\mathbf{u}}(a) = \mathbf{u}^0(a) \quad \text{for all vertices } a$$

and

$$\int_K (\widetilde{\mathbf{u}} - \mathbf{u}) = 0 \tag{4.14}$$

hold. By a standard scaling argument from K to a unique reference element, we can obtain

$$\|\mathbf{u} - \widetilde{\mathbf{u}}\|_{0,K} \le c\|\mathbf{u} - \mathbf{u}^0\|_{0,K}.$$

Hence, (4.12) holds for $\widetilde{\mathbf{u}}$. Further, we can verify (4.11) from (3.8), (3.9), (4.13) and (4.14). The proof is completed. □

Theorem 4.1. *Let* $\mathbf{u}$ *be the exact solution of (2.1) and* $\mathbf{u}_h \in U_h$ *the finite element solution of (3.10). Assume that* $\mathbf{u} \in \prod_{j=1}^{J}(H^r(\Omega_j))^2$, $w := \mu^{-1}\mathrm{curl}\,\mathbf{u} \in H^1(\Omega) \cap \prod_{j=1}^{J} H^{1+r}(\Omega_j)$ *and* $p := \mathrm{div}\,\varepsilon\mathbf{u} \in H_0^1(\Omega) \cap \prod_{j=1}^{J} H^{1+r}(\Omega_j)$, $r \in (0,1)$. *Then we have*

$$|||\mathbf{u} - \mathbf{u}_h|||_h \le ch^r\Big(\|p\|_1 + \|w\|_1 + \sum_{j=1}^{J}\|w\|_{1+r,\Omega_j} + \sum_{j=1}^{J}\|p\|_{1+r,\Omega_j} + \sum_{j=1}^{J}\|\mathbf{u}\|_{r,\Omega_j}\Big). \tag{4.15}$$

Proof. Let $\widetilde{\mathbf{u}} \in U_h$ denote the finite element interpolation of $\mathbf{u}$ given in Lemma 4.2. We have

$$c|||\widetilde{\mathbf{u}} - \mathbf{u}_h|||_h^2 \le \mathscr{A}_h(\widetilde{\mathbf{u}} - \mathbf{u}_h, \widetilde{\mathbf{u}} - \mathbf{u}_h),$$

where

$$\mathscr{A}_h(\widetilde{\mathbf{u}} - \mathbf{u}_h, \widetilde{\mathbf{u}} - \mathbf{u}_h) = \mathscr{A}_h(\widetilde{\mathbf{u}} - \mathbf{u}, \widetilde{\mathbf{u}} - \mathbf{u}_h) + \mathscr{A}_h(\mathbf{u} - \mathbf{u}_h, \widetilde{\mathbf{u}} - \mathbf{u}_h).$$

From Lemma 4.2, we obtain

$$\mathscr{A}_h(\widetilde{\mathbf{u}} - \mathbf{u}, \widetilde{\mathbf{u}} - \mathbf{u}_h) = -\lambda(\widetilde{\mathbf{u}} - \mathbf{u}, \widetilde{\mathbf{u}} - \mathbf{u}_h) \le ch^r \sum_{j=1}^{J}\|\mathbf{u}\|_{r,\Omega_j}\|\widetilde{\mathbf{u}} - \mathbf{u}_h\|_0,$$

and from Lemma 4.1 we have

$$\mathscr{A}_h(\mathbf{u} - \mathbf{u}_h, \widetilde{\mathbf{u}} - \mathbf{u}_h) \le ch^r\Big(\|p\|_1 + \|w\|_1 + \sum_{j=1}^{J}\|w\|_{1+r,\Omega_j} + \sum_{j=1}^{J}\|p\|_{1+r,\Omega_j}\Big)|||\widetilde{\mathbf{u}} - \mathbf{u}_h|||_h.$$

Hence, we obtain

$$|||\widetilde{\mathbf{u}} - \mathbf{u}_h|||_h \le ch^r\Big(\|p\|_1 + \|w\|_1 + \sum_{j=1}^{J}\|w\|_{1+r,\Omega_j} + \sum_{j=1}^{J}\|p\|_{1+r,\Omega_j} + \sum_{j=1}^{J}\|\mathbf{u}\|_{r,\Omega_j}\Big).$$

But, Lemma 4.2 and the definition (4.8) of $|||\cdot|||_h$ result in

$$|||\widetilde{\mathbf{u}} - \mathbf{u}|||_h = \|\widetilde{\mathbf{u}} - \mathbf{u}\|_0 \le ch^r \sum_{j=1}^{J}\|\mathbf{u}\|_{r,\Omega_j}.$$

Now, the bound for $|||\mathbf{u}-\mathbf{u}_h|||_h$ follows, using the triangle inequality with $|||\widetilde{\mathbf{u}}-\mathbf{u}_h|||_h$ and $|||\widetilde{\mathbf{u}}-\mathbf{u}|||_h$. This completes the proof. □

Remark 4.1. From the theory of eigenproblem in [5], when solving eigenproblem (3.12), we can conclude from Theorem 4.1 that the error bound for eigenvalues is $O(h^{2r})$.

Remark 4.2. For general piecewise smooth ε, we may consider its suitable finite element interpolation ε_h, as done in Remark 4.7 in [26]. In that case, the element-bubble space B_h in (3.1) should be replaced by the following one:

$$B_h(\varepsilon_h) = \{\mathbf{v} \in (H_0^1(\Omega))^2 : \mathbf{v}|_K \in b_K\mathbf{P}(K,\varepsilon_h), \forall K \in \mathscr{T}_h\},$$

where

$$\mathbf{P}(K,\varepsilon_h) = \text{span}\{\varepsilon_h(P_0(K))^2, (P_0(K))^2\}.$$

5. Numerical experiments

In this section, by considering a number of examples of source problem and eigenvalue problem for Maxwell's equations, we are going to illustrate the superior performance of the proposed nodal-continuous linear finite element approach. The numerical examples are divided into two subsections of source problem and eigenvalue problem, while each subsection is further divided into two subsections of homogeneous medium and nonhomogeneous medium.

5.1. Source problem

5.1.1. Homogeneous medium

We consider the time-harmonic Maxwell's equations (2.4) on an L-domain $\Omega = (-1,1)^2\backslash([0,1)\times(-1,0])$ and a cracked domain $\Omega = (-1,1)^2\backslash\{(x,y) \in \mathbb{R}^2 |\ 0 \le x < 1, y = 0\}$. The continuous variational problem is given in (2.5). The finite element problem can be stated as (3.10), with the bilinear form (3.11), while the right-hand side is replaced by $(\mathbf{J},\mathbf{v}_h) + (g, \check{R}_h(\text{div}\,\mathbf{v}_h))$. Note that $\lambda = \omega^2$ and $\mu = \varepsilon = 1$. In this subsection, we always take $\lambda = 1$.

For the L-domain problem, we take the exact solution to be

$$\mathbf{u}(x,y) = \nabla((1-x^2)(1-y^2)p(x,y)),$$

where $x = \rho\cos(\theta)$, $y = \rho\sin(\theta)$, $p(x,y) := \rho^{2/3}\sin(\frac{2}{3}\theta)$, and ρ is the distance to the origin and θ is the angular degree varying form 0 to $3\pi/2$. One can check that the exact solution $\mathbf{u}$ has a strong unbounded singularity at the origin, and it satisfies the homogeneous tangential boundary condition, $\mathbf{u}\cdot\boldsymbol{\tau} = 0$ on Γ. For simplifying the computations, we will use the uniform triangle meshes as shown in Figure 5.1 (left). To observe the convergence rate, we let the mesh size h decrease by half, i.e., $h = 1/4, 1/8, \cdots, 1/128$. Since $p \in H^{5/3-\epsilon}(\Omega)$ for any $\epsilon > 0$, it follows that $\mathbf{u} \in (H^{2/3-\epsilon}(\Omega))^2$ (cf. [27]). Thus, the predicted convergence rate for the finite element solution is approximately $2/3 \approx 0.67$. The computed results which are shown in Table 5.1 confirm this rate. The elevations and contour plots of the finite element solution $\mathbf{u}_h$ and the exact solution $\mathbf{u}$ for $h = 1/32$ are shown in Figure 5.2. We remark that, due to the unbounded singularity of the exact solution at the origin, a fraction of the graphs near the origin will not be displayed.

For the cracked domain problem, we choose $\mathbf{J}$ and g such that the exact solution is

$$\mathbf{u}(x,y) = \nabla((1-x^2)(1-y^2)q(x,y)),$$

where $q(x,y) := \rho^{1/2}\sin(\frac{1}{2}\theta)$ and θ is varying form 0 to 2π. This exact solution $\mathbf{u}$ has a strong unbounded singularity at the origin, and $\mathbf{u}\cdot\boldsymbol{\tau} = 0$ on Γ. In this case, since $q \in H^{3/2-\epsilon}(\Omega)$ for any $\epsilon > 0$, we have $\mathbf{u} \in (H^{1/2-\epsilon}(\Omega))^2$. Thus, the predicted convergence rate for the finite element solution is approximately 0.5. A typical uniform triangle mesh of the cracked domain employed in the computation is drawn in Figure 5.1 (right). Again, the computed results reported in Table 5.2 confirm this rate. The elevations and contour curves of the finite element solution $\mathbf{u}_h$ and the exact solution $\mathbf{u}$ for $h = 1/32$ are depicted in Figure 5.3.

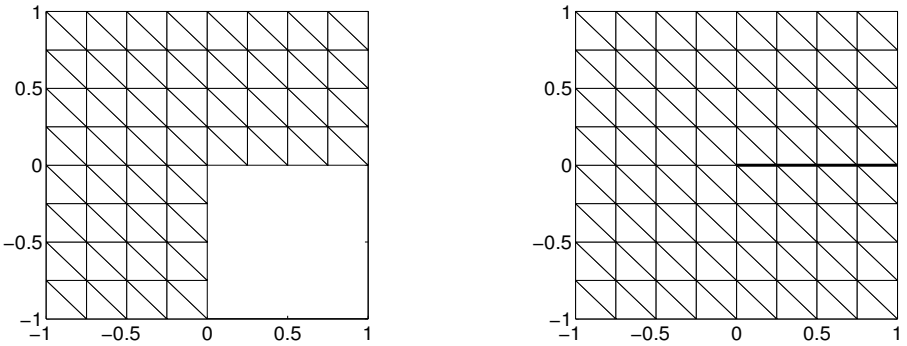

Figure 5.1. A typical uniform triangle mesh with $h = 1/4$: (left) L-domain; (right) cracked domain.

Table 5.1. Relative errors of u_{1h} and u_{2h} in the L^2 norm of the L-domain problem

$1/h$	4	8	16	32	64	128
$\frac{\|u_1-u_{1h}\|_0}{\|u_1\|_0}$	7.7325E-02	4.5382E-02	2.8208E-02	1.7723E-02	1.1158E-02	7.0280E-03
Rate	–	0.77	0.69	0.67	0.67	0.67
$\frac{\|u_2-u_{2h}\|_0}{\|u_2\|_0}$	7.7325E-02	4.5382E-02	2.8208E-02	1.7723E-02	1.1158E-02	7.0280E-03
Rate	–	0.77	0.69	0.67	0.67	0.67

Table 5.2. Relative errors of u_{1h} and u_{2h} in the L^2 norm of the cracked domain problem

$1/h$	4	8	16	32	64	128
$\frac{\|u_1-u_{1h}\|_0}{\|u_1\|_0}$	2.3850E-01	1.6608E-01	1.0982E-01	6.8315E-02	4.1182E-02	2.5361E-02
Rate	–	0.52	0.60	0.68	0.73	0.70
$\frac{\|u_2-u_{2h}\|_0}{\|u_2\|_0}$	3.2858E-01	2.2422E-01	1.5000E-01	9.7902E-02	6.3732E-02	4.2395E-02
Rate	–	0.55	0.58	0.62	0.62	0.59

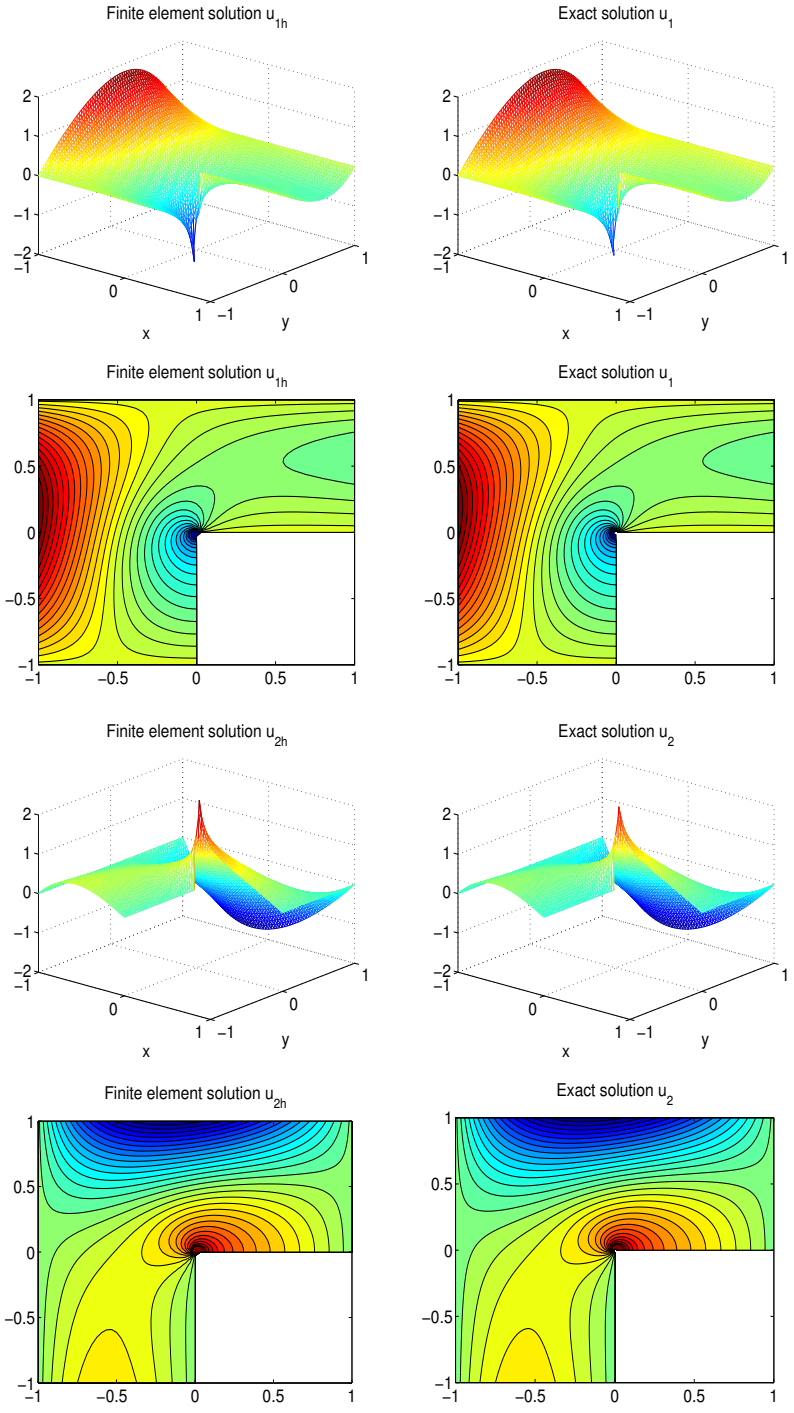

Figure 5.2. Elevations and contour curves of the finite element solution $\mathbf{u}_h = (u_{1h}, u_{2h})$ and the exact solution $\mathbf{u} = (u_1, u_2)$ for $h = 1/32$ of the L-domain problem.

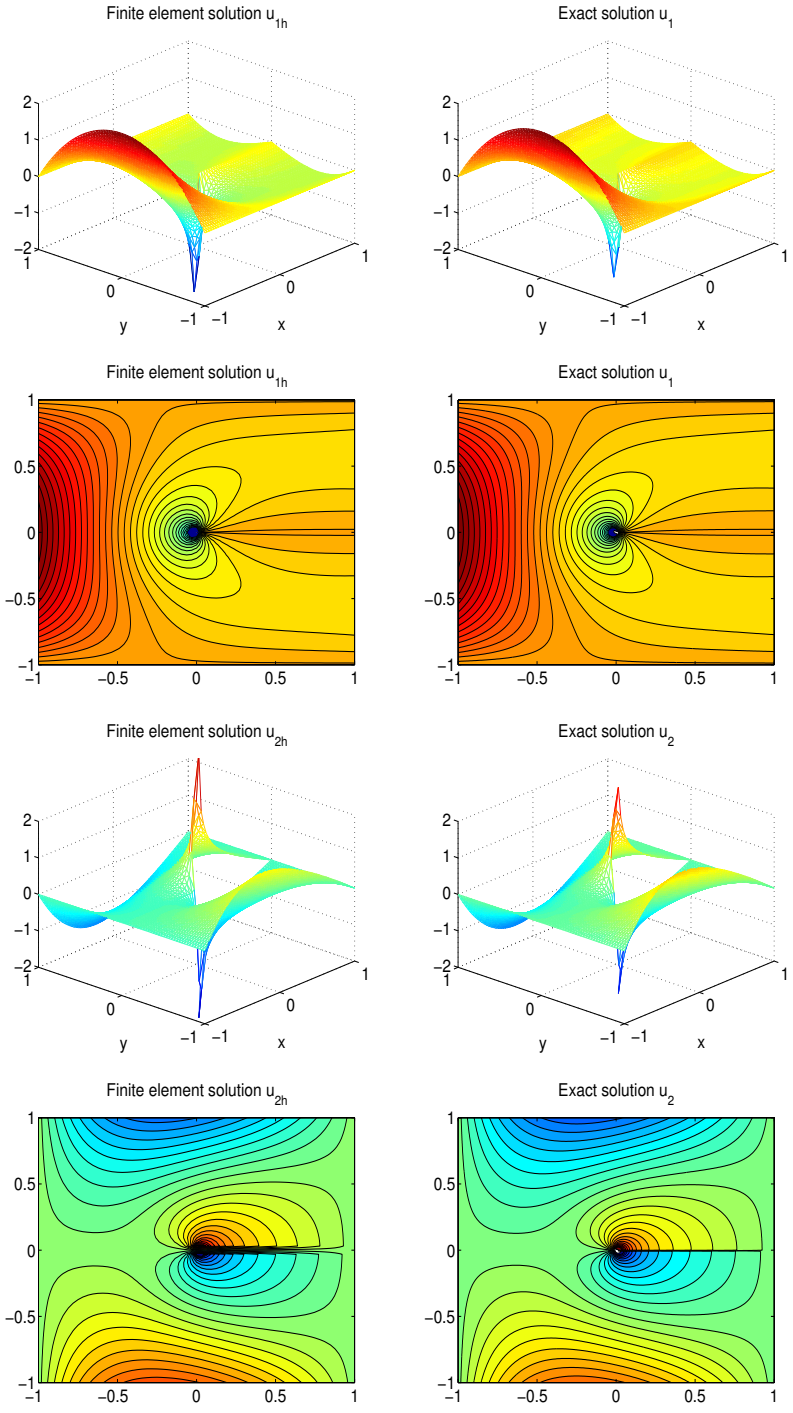

Figure 5.3. Elevations and contour curves of the finite element solution $\mathbf{u}_h = (u_{1h}, u_{2h})$ and the exact solution $\mathbf{u} = (u_1, u_2)$ for $h = 1/32$ of the cracked domain problem.

5.1.2. Nonhomogeneous medium

Given a square domain $\Omega = (-1,1)^2$, we consider the time-harmonic Maxwell's equations, with angular frequency ω^2, in a discontinuous and nonhomogeneous medium as follows:

$$\mathbf{curl}\,\mathrm{curl}\,\mathbf{u} - \omega^2\varepsilon\mathbf{u} = \mathbf{J}, \quad \mathrm{div}\,\varepsilon\mathbf{u} = 0 \quad \text{in } \Omega, \quad \mathbf{u}\cdot\boldsymbol{\tau} = \chi \quad \text{on } \Gamma. \tag{5.1}$$

Here $\mu = 1$. The coefficient ε is piecewise constant, $\varepsilon = \beta$ in $[0,1]^2$ and $[-1,0]^2$, while $\varepsilon = 1$ in $[-1,0)\times(0,1]$ and $(0,1]\times[-1,0)$. Let $\lambda := \omega^2 = 1$.

We consider the numerical example used in [41] for our purpose. Taking

$$p(x,y) = \rho^{\xi}\psi(\theta)$$

in the polar coordinate system with the variables (ρ,θ), where

$$\psi(\theta) = \begin{cases} \cos((\pi/2-\sigma)\xi)\cdot\cos((\theta-\pi/2+\alpha)\xi), & 0 \le \theta \le \pi/2, \\ \cos(\alpha\xi)\cdot\cos((\theta-\pi+\sigma)\xi), & \pi/2 \le \theta \le \pi, \\ \cos(\sigma\xi)\cdot\cos((\theta-\pi-\alpha)\xi), & \pi \le \theta \le 3\pi/2, \\ \cos((\pi/2-\alpha)\xi)\cdot\cos((\theta-3\pi/2-\sigma)\xi), & 3\pi/2 \le \theta \le 2\pi, \end{cases}$$

and the numbers ξ, α, σ and β satisfy the following nonlinear relations:

$$\begin{cases} \beta = -\tan((\pi/2-\sigma)\xi)\cdot\cot(\alpha\xi), \\ 1/\beta = -\tan(\alpha\xi)\cdot\cot(\sigma\xi), \\ \beta = -\tan(\sigma\xi)\cdot\cot((\pi/2-\alpha)\xi), \\ 0 < \xi < 2, \\ \max(0,\pi\xi-\pi) < 2\xi\alpha < \min(\pi\xi,\pi), \\ \max(0,\pi-\pi\xi) < -2\xi\sigma < \min(\pi,2\pi-\pi\xi), \end{cases}$$

then one can verify that

$$\mathrm{div}\,(\varepsilon\nabla p) = 0.$$

Since

$$p \in H^1(\Omega) \cap \prod_{j=1}^{4} H^{1+\eta}(\Omega_j), \quad \text{where } \eta < \xi,$$

if we set $\mathbf{u} := \nabla p$ to be the exact solution of (5.1) then we have

$$\mathbf{u} := \nabla p \in \prod_{j=1}^{4} (H^{\eta}(\Omega_j))^2.$$

Notice that this exact solution $\mathbf{u}$ has a strong unbounded singularity at the origin.

Now, we consider the following three cases (see Figure 5.4):

- *Case A.* $\xi = 0.5$, $\beta = 5.8284271247461907$, $\alpha = \pi/4$, $\sigma = -2.3561944901923448$.
- *Case B.* $\xi = 0.1$, $\beta = 161.4476387975881$, $\alpha = \pi/4$, $\sigma = -14.92256510455152$.
- *Case C.* $\xi = 0.02$, $\beta = 4052.1806954768103$, $\alpha = \pi/4$, $\sigma = -77.754418176347386$.

According to the regularity of $\mathbf{u}$, the predicted rate should be about η, approximately near to ξ. For *Case A*, $\xi = 0.5$, for *Case B*, $\xi = 0.1$, while, for *Case C*, $\xi = 0.02$. The numerical results reported in Tables 5.3–5.5 confirm the predictions, where we use the uniform triangulations as that shown in Figure 5.5. The contour plots of the finite element solution $\mathbf{u}_h$ for $h = 1/128$ and the exact solution $\mathbf{u}$ are depicted in Figures 5.6–5.8. Numerical results show the superior performance of the proposed nodal-continuous linear finite element approach.

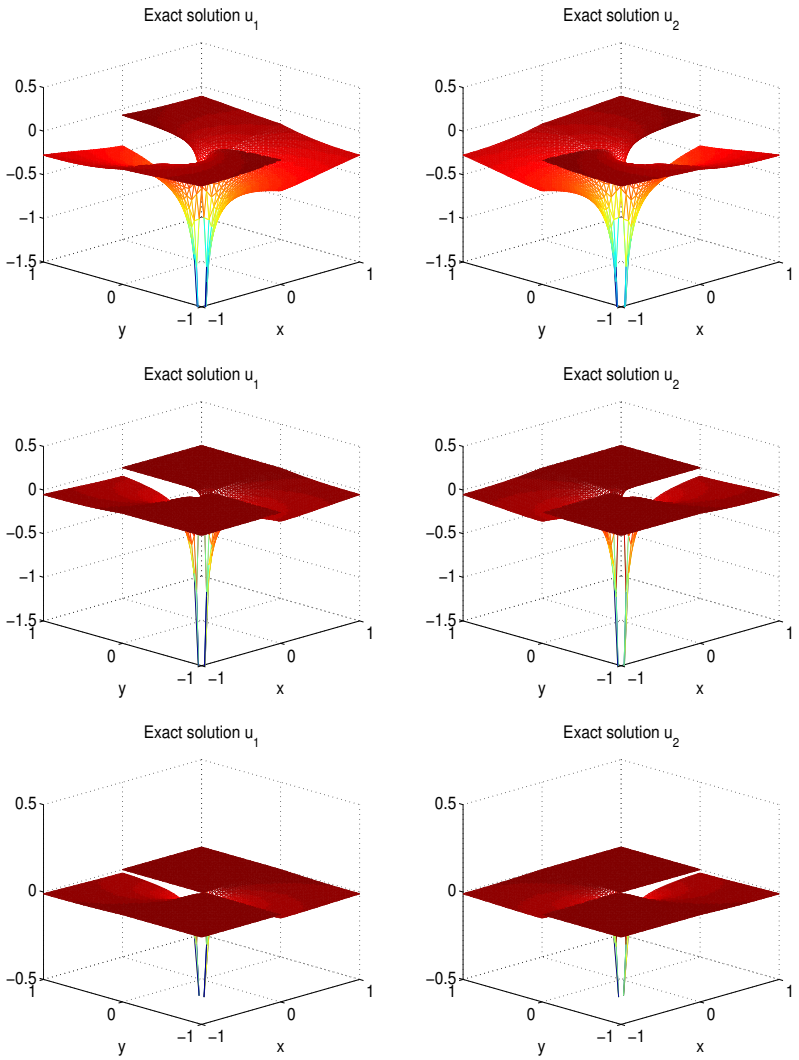

Figure 5.4. Elevations of the exact solution $\mathbf{u} = (u_1, u_2)$ of the nonhomogeneous medium problem: *Case A*, $\xi = 0.5$ (top row); *Case B*, $\xi = 0.1$ (middle row); *Case C*, $\xi = 0.02$ (bottom row).

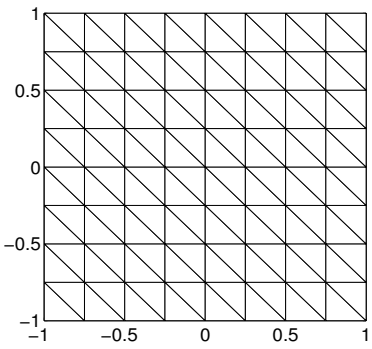

Figure 5.5. A typical uniform triangle mesh with $h = 1/4$ of the square domain Ω.

Table 5.3. Relative errors of u_{1h} and u_{2h} in the L^2 norm of the nonhomogeneous medium problem, *Case A*

$1/h$	4	8	16	32	64	128
$\frac{\|u_1-u_{1h}\|_0}{\|u_1\|_0}$	8.4969E-01	3.3310E-01	1.7622E-01	1.1774E-01	8.5445E-02	6.3163E-02
Rate	–	1.35	0.92	0.58	0.46	0.44
$\frac{\|u_2-u_{2h}\|_0}{\|u_2\|_0}$	8.4969E-01	3.3310E-01	1.7622E-01	1.1774E-01	8.5445E-02	6.3163E-02
Rate	–	1.35	0.92	0.58	0.46	0.44

Table 5.4. Relative errors of u_{1h} and u_{2h} in the L^2 norm of the nonhomogeneous medium problem, *Case B*

$1/h$	4	8	16	32	64	128
$\frac{\|u_1-u_{1h}\|_0}{\|u_1\|_0}$	5.6533E-01	5.4702E-01	4.6614E-01	4.2381E-01	3.8665E-01	3.5393E-01
Rate	–	0.05	0.23	0.14	0.13	0.13
$\frac{\|u_2-u_{2h}\|_0}{\|u_2\|_0}$	5.6533E-01	5.4702E-01	4.6614E-01	4.2381E-01	3.8665E-01	3.5393E-01
Rate	–	0.05	0.23	0.14	0.13	0.13

Table 5.5. Relative errors of u_{1h} and u_{2h} in the L^2 norm of the nonhomogeneous medium problem, *Case C*

$1/h$	4	8	16	32	64	128
$\frac{\|u_1-u_{1h}\|_0}{\|u_1\|_0}$	6.5462E-01	6.1066E-01	5.7082E-01	5.3611E-01	5.0594E-01	4.8034E-01
Rate	–	0.10	0.10	0.09	0.08	0.07
$\frac{\|u_2-u_{2h}\|_0}{\|u_2\|_0}$	6.5462E-01	6.1066E-01	5.7082E-01	5.3611E-01	5.0594E-01	4.8034E-01
Rate	–	0.10	0.10	0.09	0.08	0.07

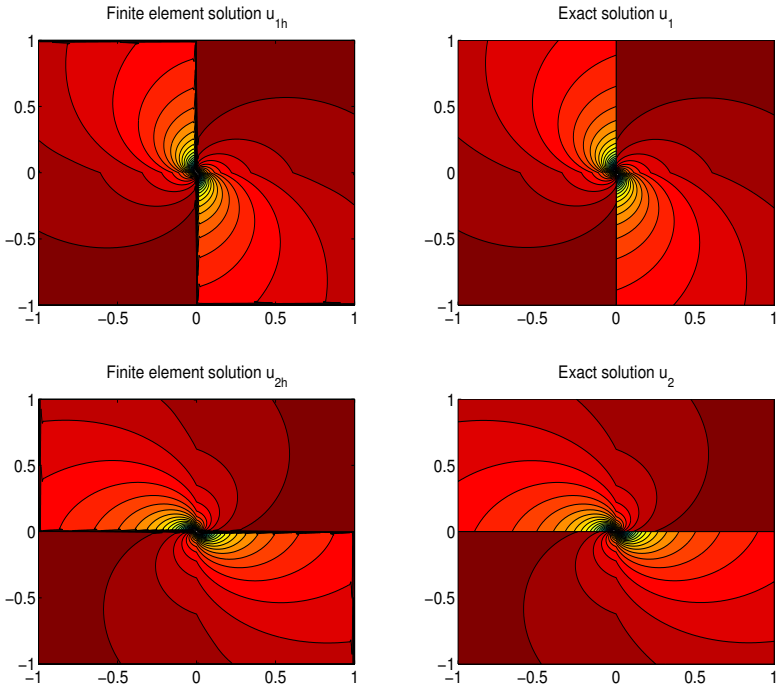

Figure 5.6. Contour plots of the finite element solution $\mathbf{u}_h = (u_{1h}, u_{2h})$ for $h = 1/128$ and the exact solution $\mathbf{u} = (u_1, u_2)$ of the nonhomogeneous medium problem, *Case A*, $\xi = 0.5$.

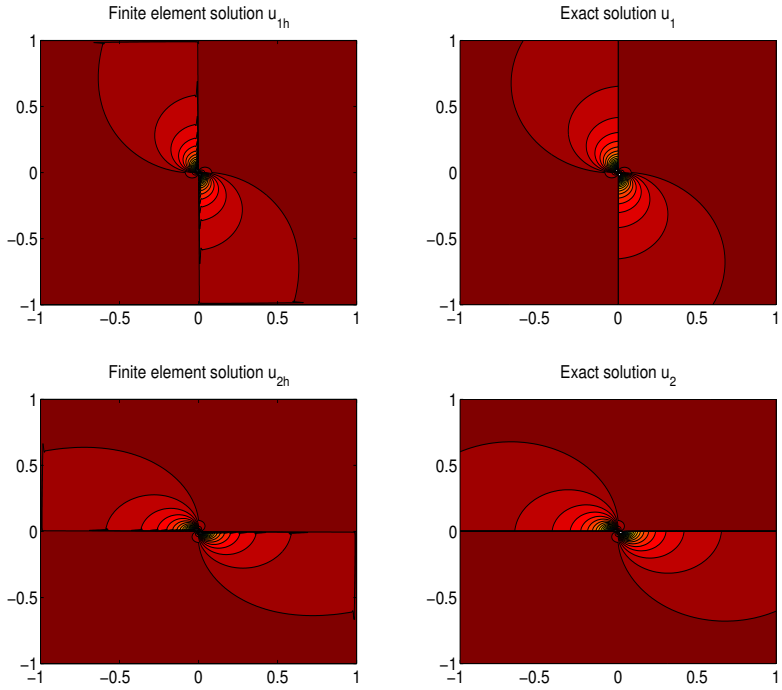

Figure 5.7. Contour plots of the finite element solution $\mathbf{u}_h = (u_{1h}, u_{2h})$ for $h = 1/128$ and the exact solution $\mathbf{u} = (u_1, u_2)$ of the nonhomogeneous medium problem, *Case B*, $\xi = 0.1$.

5.2. Eigenvalue problem

In this subsection, we shall seek the finite element solutions of the Maxwell eigenvalue problem (3.21). Both the homogeneous medium and the discontinuous nonhomogeneous medium will be studied. As in the previous subsection, we use the uniform triangle meshes. We compute the eigenvalues by the following 'shift' formulation: *Find* $\lambda_h = 1+\omega_h^2$ *and* $\mathbf{u}_h \in U_h$, $\mathbf{u}_h \neq \mathbf{0}$, *such that*

$$(R_h(\mu^{-1}\text{curl } \mathbf{u}_h), R_h(\mu^{-1}\text{curl } \mathbf{v}_h))_{0,\mu,h} + (\check{R}_h(\text{div } \varepsilon\mathbf{u}_h), \check{R}_h(\text{div } \varepsilon\mathbf{v}_h))_{0,h} + (\varepsilon\mathbf{u}_h, \mathbf{v}_h) = \lambda_h(\varepsilon\mathbf{u}_h, \mathbf{v}_h) \quad \forall \mathbf{v}_h \in U_h. \tag{5.2}$$

5.2.1. Homogeneous medium

Taking $\mu = \varepsilon = 1$, we first consider the eigenvalue problem on the L-domain $\Omega = (-1, 1)^2 \backslash ([0, 1) \times (-1, 0])$. We will take the nonzero eigenvalues provided by Monique Dauge at her personal page

$$\texttt{http://perso.univ-rennes1.fr/monique.dauge/benchmax.html}$$

as the benchmark. For example, the first two nonzero eigenvalues given there are

$$\omega_1^2 = 1.47562182408 \quad \text{and} \quad \omega_2^2 = 3.53403136678.$$

The corresponding eigenfunctions are $\mathbf{u}^1 \in (H^{2/3-\epsilon}(\Omega))^2$ and $\mathbf{u}^2 \in (H^{4/3-\epsilon}(\Omega))^2$, for any $\epsilon > 0$ (cf. [20]). Then the predicted convergence rate of the nonzero finite element eigenvalue ω_h^2 to ω^2 is as follows: for ω_1^2, it is approximately $2 \times 2/3 \approx 1.33$, while, for ω_2^2, it is 2. Note that for the second eigenvalue the convergence rate is not approximately $2 \times 4/3$ from the theoretical analysis, because here we only use the linear finite elements. The numerical results reported in Table 5.6 confirm the predicted rates of convergence. One can find that our method can approximate the eigenvalues very well, even for a rather coarse grid. Moreover, we can accurately approximate the other three nonzero eigenvalues given by Monique Dauge as well. The convergence rates are still of second order, which is optimal for smooth eigenfunctions. We omit the details here.

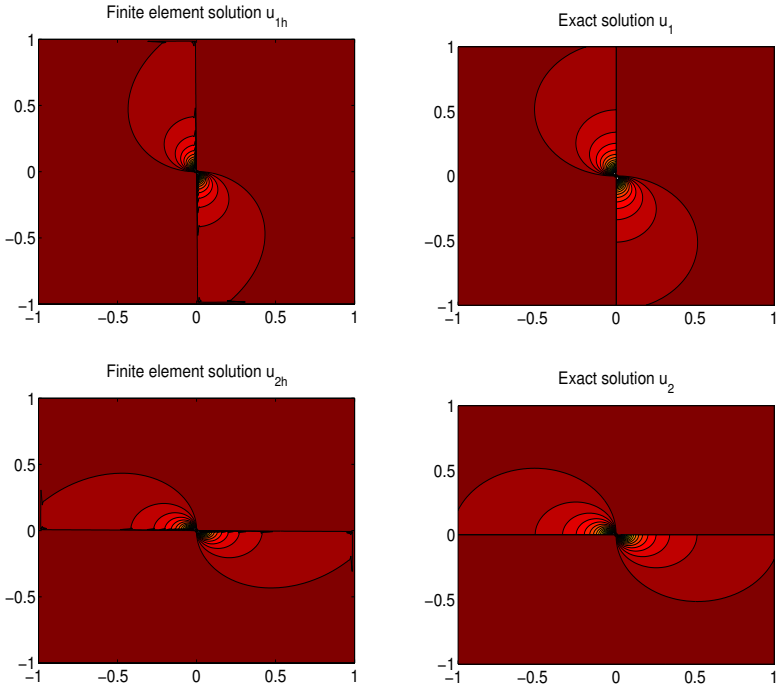

Figure 5.8. Contour plots of the finite element solution $\mathbf{u}_h = (u_{1h}, u_{2h})$ for $h = 1/128$ and the exact solution $\mathbf{u} = (u_1, u_2)$ of the nonhomogeneous medium problem, *Case C*, $\xi = 0.02$.

Table 5.6. Relative errors and rates of convergence of the first two nonzero finite element eigenvalues of the eigenvalue problem on the L-domain

ω^2	$1/h$	ω_h^2	$\lvert\omega^2 - \omega_h^2\rvert/\lvert\omega^2\rvert$	Rate
1.47562182408	4	1.48831405934	8.6013E-03	–
	8	1.48334479049	5.2337E-03	0.72
	16	1.47934670251	2.5243E-03	1.05
	32	1.47726489565	1.1135E-03	1.18
	64	1.47631519067	4.6988E-04	1.24
	128	1.47590733958	1.9349E-04	1.28
3.53403136678	4	3.39884629080	3.8252E-02	–
	8	3.49993848487	9.6470E-03	1.99
	16	3.52548553846	2.4182E-03	2.00
	32	3.53189291161	6.0510E-04	2.00
	64	3.53349654404	1.5134E-04	2.00
	128	3.53389763603	3.7841E-05	2.00

Table 5.7. Relative errors and rates of convergence of the first two nonzero finite element eigenvalues of the eigenvalue problem on the cracked domain

ω^2	$1/h$	ω_h^2	$\lvert\omega^2-\omega_h^2\rvert/\lvert\omega^2\rvert$	Rate
1.03407400850	4	1.09324290753	5.7219E-02	–
	8	1.06617286421	3.1041E-02	0.88
	16	1.05070135673	1.6079E-02	0.95
	32	1.04252667113	8.1741E-03	0.98
	64	1.03833444080	4.1200E-03	0.99
	128	1.03621265987	2.0682E-03	0.99
2.46740110027	4	2.41156768316	2.2628E-02	–
	8	2.45340321169	5.6731E-03	2.00
	16	2.46389719213	1.4201E-03	2.00
	32	2.46652457342	3.5524E-04	2.00
	64	2.46718189841	8.8839E-05	2.00
	128	2.46734629070	2.2213E-05	2.00

Next, we consider the eigenvalue problem on the cracked domain defined by $\Omega = (-1,1)^2\backslash\{(x,y) \in \mathbb{R}^2 |\ 0 \le x < 1, y = 0\}$. Again, we take the first two nonzero eigenvalues from Monique Dauge's page as the benchmark as follows:

$$\omega_1^2 = 1.03407400850 \quad \text{and} \quad \omega_2^2 = 2.46740110027.$$

The corresponding eigenfunctions are given by $\mathbf{u}^1 \in (H^{1/2-\epsilon}(\Omega))^2$ for any $\epsilon > 0$ and $\mathbf{u}^2 \in (H^1(\Omega))^2$. So, the predicted convergence rate of the nonzero finite element eigenvalue ω_h^2 to ω^2 is as follows: for ω_1^2, it is approximately 1, while, for ω_2^2, it is 2. The computed results are collected in Table 5.7, which confirm the predicted rates of convergence. We remark that we can accurately approximate the other eight nonzero eigenvalues given by Monique Dauge with convergence rates of second order.

5.2.2. Nonhomogeneous medium

We now consider the eigenvalue problem with the nonhomogeneous medium on the square domain $\Omega = (-1,1)^2$. The coefficients ε are given by

$$\varepsilon = \begin{cases} \varepsilon_1, & (x,y) \in [-1,0]^2 \bigcup [0,1]^2, \\ 1, & \text{otherwise}, \end{cases}$$

and $\mu = 1$. For comparison with the benchmark results reported at Monique Dauge's personal page mentioned above, where the Maxwell's eigenvalues coincide with the nonzero Neumann eigenvalues of the magnetic problem, we consider the following various values of ε_1: $\varepsilon_1 = 0.5, 0.1, 0.01, 10^{-8}$.

In Table 5.8, the computed results using $h = 1/128$ for each ε_1 are compared with those ten nonzero eigenvalues provided by Monique Dauge. We see that the approximations show good agreements, except for the third eigenvalue $\omega^2 = 15.536981653110$ and the seventh eigenvalue $\omega^2 = 29.646623662180$ for the case of $\varepsilon_1 = 0.01$. At her personal page, Monique Dauge indicated that for these two eigenvalues, only three digits are expected to be correct, although she used the adaptive Galerkin computations with high degree polynomials. Here, we study the convergence behavior of these two eigenvalues in more details. The results are reported in Table 5.9, from which we can find that the rates of convergence are approximately 0.2 and 0.4, respectively.

6. Concluding remarks

In this paper, we have proposed and analyzed a new nodal-continuous finite element method for numerically solving the curlcurl-graddiv problem, with mass-lumping linear finite element L^2 projections applied to the curl and the divergence operators. The nodal-continuous Lagrange linear elements, enriched with one element bubble per element, are employed. The method is designed for the general source and eigenvalue problems, and particularly the discontinuous

Table 5.8. Comparison of the nonzero finite element eigenvalues ω_h^2 for $h = 1/128$ with the benchmark values ω^2 of the eigenvalue problem with a nonhomogeneous medium for various ε_1

	ω^2	ω_h^2	$\lvert\omega^2 - \omega_h^2\rvert/\lvert\omega^2\rvert$
$\varepsilon_1 = 0.5$	3.317548763415	3.317172554712	1.1340E-04
	3.366324157260	3.365533633122	2.3483E-04
	6.186389562488	6.186032830042	5.7664E-05
	13.92632333103	13.92332332254	2.1542E-04
	15.08299096123	15.07977426632	2.1327E-04
	15.77886590819	15.77557882954	2.0832E-04
	18.64329693686	18.64123058671	1.1084E-04
	25.79753111031	25.78666659986	4.2115E-04
	29.85240067684	29.84238360527	3.3555E-04
	30.53785871253	30.52848014629	3.0711E-04
$\varepsilon_1 = 0.1$	4.533851871670	4.533227774037	1.3765E-04
	6.250332186603	6.269605774928	3.0836E-03
	7.037074196012	7.036488154255	8.3279E-05
	22.34193733540	22.33512948867	3.0471E-04
	22.67919225111	22.67200297928	3.1700E-04
	26.09520456863	26.09314572298	7.8897E-05
	26.50900637498	26.50185477490	2.6978E-04
	40.48783516243	40.45915477245	7.0837E-04
	42.65069898070	42.63023003767	4.7992E-04
	55.88227467094	55.84715453632	6.2847E-04
$\varepsilon_1 = 0.01$	4.893193324891	4.892887406014	6.2519E-05
	7.206675422492	7.206110018514	7.8456E-05
	15.53698165311	18.91602088454	2.1748E-01
	24.46225024727	24.45741961792	1.9747E-04
	24.48745601340	24.48095713851	2.6540E-04
	27.75724058215	27.74917832668	2.9046E-04
	29.64662366218	32.57750242546	9.8860E-02
	44.24890377211	44.23326910535	3.5333E-04
	44.43521693426	44.41935154387	3.5705E-04
	63.59570343398	63.55990887597	5.6285E-04
$\varepsilon_1 = 10^{-8}$	4.934802158785	4.934552567656	5.0578E-05
	7.225211232692	7.224615002304	8.2521E-05
	24.67400464789	24.66764161372	2.5788E-04
	24.67401079360	24.66945695481	1.8456E-04
	24.67401081785	24.66945935504	1.8446E-04
	27.86885061384	27.86068446997	2.9302E-04
	44.41321964155	44.39827958750	3.3639E-04
	44.74562877982	44.73090364601	3.2909E-04
	64.15240830542	64.11440151855	5.9245E-04
	64.15242807291	64.11661006660	5.5833E-04

Table 5.9. Relative errors and rates of convergence of the third and seventh nonzero eigenvalues of the nonhomogeneous medium eigenvalue problem with $\varepsilon_1 = 0.01$

ω^2	$1/h$	ω_h^2	$\lvert\omega^2 - \omega_h^2\rvert/\lvert\omega^2\rvert$	Rate
15.53698165311	8	21.11621041687	3.5909E-01	–
	16	20.87862629506	3.4380E-01	0.06
	32	20.24432077557	3.0298E-01	0.18
	64	19.56823511999	2.5946E-01	0.22
	128	18.91602088454	2.1748E-01	0.25
29.64662366218	8	38.79632947426	3.0863E-01	–
	16	36.72877705976	2.3889E-01	0.37
	32	34.91920856254	1.7785E-01	0.43
	64	33.57692913332	1.3257E-01	0.42
	128	32.57750242546	9.8860E-02	0.42

and nonhomogeneous medium has been taken into account. Some error estimates are given and a number of numerical examples have shown that the proposed method is suitable for problems with singular solution, which are typically due to re-entrant corners of Ω and discontinuous media. For such a singular and non-H^1 solution of H^r-regularity, we have tested several values of the regularity exponent r in the interval $(0, 1)$ for source and eigenvalue problems in homogeneous and discontinuous nonhomogeneous media. We have seen that the proposed method produces correctly convergent nodal-continuous finite element solutions, at the convergence rate being optimal with respect to the regularity of the true solution.

Appendix A

In this appendix, we show that the proposed method (3.10) is essentially a nodal-continuous linear finite element method, since we can eliminate the element-bubbles in U_h from (3.10) using the static condensation procedure (cf. [31]). Assume that $\mathbf{u}_h = \mathbf{u}_1 + \mathbf{u}_b \in ((V_h)^2 \cap H_0(\mathrm{curl}\,;\Omega)) + B_h$, where $\mathbf{u}_1$ is the linear part and $\mathbf{u}_b$ is the bubble part. Then $\mathbf{u}_b$ can be expressed as $\mathbf{u}_b = \sum_{K\in\mathscr{T}_h} \mathbf{c}_K^u b_K$, where $b_K := \lambda_1\lambda_2\lambda_3 \in B_h$ is the K-element bubble function with compact support in K and $\mathbf{c}_K^u$ is the corresponding coefficient vector. It is easily to verify that the nodal-continuous finite element method (3.10) is equivalent to *finding* $\mathbf{u}_h \in U_h$ *such that*

$$\begin{cases} \mathcal{A}_h(\mathbf{u}_h, \mathbf{v}_1) = (\varepsilon\mathbf{f}, \mathbf{v}_1) \quad \forall \mathbf{v}_1 \in (V_h)^2 \cap H_0(\mathrm{curl}\,;\Omega), \\ \mathcal{A}_h(\mathbf{u}_h, \mathbf{c}_K b_K) = (\varepsilon\mathbf{f}, \mathbf{c}_K b_K) \quad \forall \mathbf{c}_K b_K \in B_h. \end{cases} \tag{A.1}$$

From the second equation in (A.1) with the properties of the projection operators R_h and $\breve{R}_h$, we have

$$\begin{aligned} &(R_h(\mu^{-1}\mathrm{curl}\,\mathbf{u}_1), R_h(\mu^{-1}\mathrm{curl}\,\mathbf{c}_K b_K))_{0,\mu,h} + (R_h(\mu^{-1}\mathrm{curl}\sum_{K\in\mathscr{T}_h}\mathbf{c}_K^u b_K), R_h(\mu^{-1}\mathrm{curl}\,\mathbf{c}_K b_K))_{0,\mu,h} \\ &+(\breve{R}_h(\mathrm{div}\,\varepsilon\mathbf{u}_1), \breve{R}_h(\mathrm{div}\,\varepsilon\mathbf{c}_K b_K))_{0,h} + (\breve{R}_h(\mathrm{div}\,\varepsilon\sum_{K\in\mathscr{T}_h}\mathbf{c}_K^u b_K), \breve{R}_h(\mathrm{div}\,\varepsilon\mathbf{c}_K b_K))_{0,h} \\ &-\lambda\,(\varepsilon\mathbf{u}_1, \mathbf{c}_K b_K) - \lambda\,(\varepsilon\sum_{K\in\mathscr{T}_h}\mathbf{c}_K^u b_K, \mathbf{c}_K b_K) = (\varepsilon\mathbf{f}, \mathbf{c}_K b_K) \quad \forall \mathbf{c}_K b_K \in B_h. \end{aligned} \tag{A.2}$$

Since $\mathbf{u}_1$ is piecewise linear, from (3.8) and (3.9) we have

$$\begin{aligned} (R_h(\mu^{-1}\mathrm{curl}\,\mathbf{u}_1), R_h(\mu^{-1}\mathrm{curl}\,\mathbf{c}_K b_K))_{0,\mu,h} &= (\mu^{-1}\mathrm{curl}\,\mathbf{u}_1, R_h(\mu^{-1}\mathrm{curl}\,\mathbf{c}_K b_K))_{0,\mu,h} \\ &= (\mu^{-1}\mathrm{curl}\,\mathrm{curl}\,\mathbf{u}_1, \mathbf{c}_K b_K) = 0 \quad \forall \mathbf{c}_K b_K \in B_h \end{aligned}$$

and

$$\begin{aligned} (\breve{R}_h(\mathrm{div}\,\varepsilon\mathbf{u}_1), \breve{R}_h(\mathrm{div}\,\varepsilon\mathbf{c}_K b_K))_{0,h} &= (\mathrm{div}\,\varepsilon\mathbf{u}_1, \breve{R}_h(\mathrm{div}\,\varepsilon\mathbf{c}_K b_K))_{0,h} \\ &= -(\varepsilon\nabla\,\mathrm{div}\,\varepsilon\mathbf{u}_1, \mathbf{c}_K b_K) = 0 \quad \forall \mathbf{c}_K b_K \in B_h. \end{aligned}$$

Substituting the above identities into (A.2), we obtain

$$\begin{aligned}&(R_h(\mu^{-1}\mathrm{curl}\sum_{K\in\mathscr{T}_h}\mathbf{c}_K^u b_K), R_h(\mu^{-1}\mathrm{curl}\,\mathbf{c}_K b_K))_{0,\mu,h} + (\check{R}_h(\mathrm{div}\,\varepsilon\sum_{K\in\mathscr{T}_h}\mathbf{c}_K^u b_K), \check{R}_h(\mathrm{div}\,\varepsilon\mathbf{c}_K b_K))_{0,h}\\ &-\lambda\,(\varepsilon\sum_{K\in\mathscr{T}_h}\mathbf{c}_K^u b_K, \mathbf{c}_K b_K) = (\varepsilon\mathbf{f}, \mathbf{c}_K b_K) + \lambda\,(\varepsilon\mathbf{u}_1, \mathbf{c}_K b_K)\quad \forall \mathbf{c}_K b_K \in B_h.\end{aligned} \tag{A.3}$$

Now, for each $K \in \mathscr{T}_h$, taking $\mathbf{c}_K = (1,0)^\top$ and $\mathbf{c}_K = (0,1)^\top$ in (A.3), one can solve the 2-component vector $\mathbf{c}_K^u$ by considering the resultant 2×2 linear system. We formally denote $\mathbf{c}_K^u$ by $\mathbf{c}_K^u = \mathcal{F}(\mathbf{f}, \mathbf{u}_1, K)$. Putting these bubble coefficients $\{\mathbf{c}_K^u : K \in \mathscr{T}_h\}$ into the first equation of (A.1), the nodal-continuous finite element method (3.10) becomes to *find* $\mathbf{u}_1 \in (V_h)^2 \cap H_0(\mathrm{curl}\,;\Omega)$ *such that*

$$\begin{aligned}&(R_h(\mu^{-1}\mathrm{curl}\,\mathbf{u}_1), R_h(\mu^{-1}\mathrm{curl}\,\mathbf{v}_1))_{0,\mu,h} + (\check{R}_h(\mathrm{div}\,\varepsilon\mathbf{u}_1), \check{R}_h(\mathrm{div}\,\varepsilon\mathbf{v}_1))_{0,h} - \lambda\,(\varepsilon\mathbf{u}_1, \mathbf{v}_1)\\ &+(R_h(\mu^{-1}\mathrm{curl}\sum_{K\in\mathscr{T}_h}\mathcal{F}(\mathbf{f},\mathbf{u}_1,K)b_K), R_h(\mu^{-1}\mathrm{curl}\,\mathbf{v}_1))_{0,\mu,h} + (\check{R}_h(\mathrm{div}\,\varepsilon\sum_{K\in\mathscr{T}_h}\mathcal{F}(\mathbf{f},\mathbf{u}_1,K)b_K), \check{R}_h(\mathrm{div}\,\varepsilon\mathbf{v}_1))_{0,h}\\ &-\lambda(\varepsilon\sum_{K\in\mathscr{T}_h}\mathcal{F}(\mathbf{f},\mathbf{u}_1,K)b_K, \mathbf{v}_1) = (\varepsilon\mathbf{f}, \mathbf{v}_1)\quad \forall \mathbf{v}_1 \in (V_h)^2 \cap H_0(\mathrm{curl}\,;\Omega),\end{aligned} \tag{A.4}$$

which is essentially a nodal-continuous linear finite element method.

Acknowledgments

The authors would like to thank two anonymous referees for their valuable comments and suggestions that improved the presentation of this paper. The work of Huo-Yuan Duan was partially supported by the National Natural Science Foundation of China under the grants 11071132 and 11171168, the Research Fund for the Doctoral Program of Higher Education of China under grants 20100031110002 and 20120031110026, and the Scientific Research Foundation for the Returned Overseas Chinese Scholars, State Education Ministry. The work of Suh-Yuh Yang was partially supported by the National Science Council of Taiwan under the grant NSC 101-2115-M-008-008-MY2.

References

[1] R. A. Adams, *Sobolev Spaces,* Academic Press, New York, 1975.

[2] C. Amrouche, C. Bernardi, M. Dauge, and V. Girault, Vector potentials in three-dimensional non-smooth domains, *Math. Methods Appl. Sci.,* 21 (1998), pp. 823-864.

[3] F. Assous, P. Ciarlet Jr., and J. Segré, Numerical solution to the time-dependent Maxwell equations in two-dimensional singular domain: the singular complement method, *J. Comput. Phys.,* 161 (2000), pp. 218-249.

[4] F. Assous, P. Ciarlet Jr., and E. Sonnendrücker, Resolution of the Maxwell equations in a domain with reentrant corners, *Math. Modell. Numer. Anal.,* 32 (1998), pp. 359-389.

[5] I. Babuška and J. Osborn, Eigenvalue problems, in *Handbook of Numerical Analysis, Vol II,* P. G. Ciarlet and J. L. Lions, Eds., North-Holland, Amsterdam, 1991, pp. 641-787.

[6] S. Badia and R. Codina, A nodal-based finite element approximation of the Maxwell problem suitable for singular solutions, *SIAM J. Numer. Anal.,* 50 (2012), pp. 398-417.

[7] M. Birman and M. Solomyak, L^2-theory of the Maxwell operator in arbitrary domains, *Russ. Math. Surv.,* 42 (1987), pp. 75-96.

[8] A. Bonito and J.-L. Guermond, Approximation of the eigenvalue problem for the time-harmonic Maxwell system by continuous Lagrange finite elements, *Math. Comput.,* 80 (2011), pp. 1887-1910.

[9] A.-S. Bonnet-Ben Dhia, C. Hazard, and S. Lohrengel, A singular field method for the solution of Maxwell's equations in polyhedral domains, *SIAM J. Appl. Math.,* 59 (1999), pp. 2028-2044.

[10] A. Bossavit, *Computational Electromagnetism: Variational Formulations, Complementarity, Edge Elements,* Academic Press, New York, 1998.

[11] J. Bramble and J. Pasciak, A new approximation technique for div-curl systems, *Math. Comp.,* 73 (2004), pp. 1739-1762.

[12] S. C. Brenner, F.-Y. Li, and L.-Y. Sung, A locally divergence-free interior penalty method for two-dimensional curl-curl problems, *SIAM J. Numer. Anal.,* 46 (2008), pp. 1190-1211.

[13] S. C. Brenner and L. R. Scott, *The Mathematical Theory of Finite Element Methods,* Springer-Verlag, Berlin, 1996.

[14] A. Buffa, P. Ciarlet Jr., and E. Jamelot, Solving electromagnetic eigenvalue problems in polyhedral domains, *Numer. Math.,* 113 (2009), pp. 497-518.

[15] M. Cessenat, *Mathematical Methods in Electromagnetism: Linear Theory and Applications,* World Scientific, River Edge, NJ, 1996.

[16] P. G. Ciarlet, *The Finite Element Method for Elliptic Problems,* North-Holland Publishing Company, Amsterdam, 1978.

[17] P. Clément, Approximation by finite element functions using local regularization, *RAIRO Numer. Anal.,* 9 (1975), pp. 77-84.

[18] M. Costabel, A coercive bilinear form for Maxwell's equations, *J. Math. Anal. Appl.,* 157 (1991), pp. 527-541.
[19] M. Costabel, A remark on the regularity of solutions of Maxwell's equations on Lipschitz domains, *Math. Models Methods Appl. Sci.,* 12 (1990), pp. 365-368.
[20] M. Costabel and M. Dauge, Computation of resonance frequencies for Maxwell equations in non-smooth domains, in *Lecture Notes in Computational Science and Engineering, Vol. 31,* M. Ainsworth, P. Davies, D. Duncan, P. Martin, B. Rynne, Eds., Springer-Verlag, Berlin, 2003, pp. 125-161.
[21] M. Costabel and M. Dauge, Weighted regularization of Maxwell equations in polyhedral domains, *Numer. Math.,* 93 (2002), pp. 239-277.
[22] M. Costabel and M. Dauge, Singularities of electromagnetic fields in polyhedral domains, *Arch. Rational Mech. Anal.,* 151 (2000), pp. 221-276.
[23] M. Costabel and M. Dauge, Maxwell and Lamé eigenvalues on polyhedra, *Math. Meth. Appl. Sci.,* 22 (1999), pp. 243-258.
[24] M. Costabel, M. Dauge, and S. Nicaise, Singularities of Maxwell interface problems, *Math. Modell. Numer. Anal.,* 33 (1999), pp. 627-649.
[25] H. Y. Duan, F. Jia, P. Lin, and R. C. E. Tan, The local L^2 projected C^0 finite element method for Maxwell problem, *SIAM J. Numer. Anal.,* 47 (2009), pp. 1274-1303.
[26] H. Y. Duan, P. Lin, P. Saikrishnan, and R. C. E. Tan, A least squares finite element method for the magnetostatic problem in a multiply-connected Lipschitz domain, *SIAM J. Numer. Anal.,* 45 (2007), pp. 2537-2563.
[27] H. Y. Duan, P. Lin, and R. C. E. Tan, C^0 elements for generalized indefinite Maxwell's equations, *Numer. Math.,* 122 (2012), pp. 61-99.
[28] H. Y. Duan, P. Lin, and R. C. E. Tan, Analysis of a continuous finite element method for $H(curl, div)$-elliptic interface problem, *Numer. Math.,* 123 (2013), pp. 671-707.
[29] H. Y. Duan, P. Lin, and R. C. E. Tan, Error estimates for a vectorial second-order elliptic eigenproblem by the local L^2 projected C^0 finite element method, *SIAM J. Numer. Anal.,* 51 (2013), pp. 1678-1714.
[30] C. Farhat, I. Harari, and L. P. Franca, The discontinuous enrichment method, *Comput. Methods Appl. Mech. Engrg.,* 190 (2001), pp. 6455-6479.
[31] L. P. Franca and C. Farhat, Bubble functions prompt unusual stabilized finite element methods, *Comput. Methods Appl. Mech. Engrg.*, 123 (1995), pp. 299-308.
[32] V. Girault and P. A. Raviart, *Finite Element Methods for Navier-Stokes Equations: Theory and Algorithms,* Springer-Verlag, Berlin, 1986.
[33] P. Grisvard, *Boundary Value Problems in Non-Smooth Domains,* University of Maryland, Dept. of Mathematics, Lecture Notes no. 19, 1980.
[34] C. Hazard and M. Lenoir, On the solution of time-harmonic scattering problems for Maxwell's equations, *SIAM J. Math. Anal.,* 27 (1996), pp. 1597-1630.
[35] C. Hazard and S. Lohrengel, A singular field method for Maxwell's equations: numerical aspects for 2D magnetostatics, *SIAM J. Numer. Anal.,* 40 (2003), pp. 1021-1040.
[36] R. Hiptmair, Finite elements in computational electromagnetism, *Acta Numerica,* 2002, pp. 237-339.
[37] T. J. R. Hughes, Multiscale phenomena: Greens functions, the Dirichlet-to-Neumann formulation, subgrid scale models, bubbles and the origins of stabilized methods, *Comput. Methods Appl. Mech. Engrg.,* 127 (1995), pp. 387-401.
[38] J. M. Jin, *The Finite Element Method in Electromagnetics, 2nd Ed.*, John Wiley & Sons, New York, 2002.
[39] E. J. Lee and T. A. Manteuffel, FOSLL* method for the eddy current problem with three-dimensional edge singularities, *SIAM J. Numer. Anal.,* 45 (2007), pp. 787-809.
[40] P. Monk, *Finite Element Methods for Maxwell Equations,* Clarendon Press, Oxford, 2003.
[41] P. Morin, R. H. Nochetto, and K. G. Siebert, Data oscillation and convergence of adaptive FEM, *SIAM J. Numer. Anal.,* 38 (2001), pp. 466-488.
[42] L. R. Scott and S. Zhang, Finite element interpolation of nonsmooth functions satisfying boundary conditions, *Math. Comp.,* 54 (1990), pp. 483-493.
[43] V. Thomée, *Galerkin Finite Element Methods for Parabolic Problems,* Springer-Verlag, Berlin, 1997.